Quaternary Research 82 (2014) 518–532

Contents lists available at ScienceDirect

Quaternary Research

journal homepage: www.elsevier.com/locate/yqres

Taxonomic overview and tusk growth analyses of Ziegler Reservoir proboscideans

Daniel C. Fisher [a,b,*], Michael D. Cherney [a,b], Cody Newton [c,d], Adam N. Rountrey [a,e], Zachary T. Calamari [a,b,f], Richard K. Stucky [c], Carol Lucking [c], Lesley Petrie [g]

[a] Museum of Paleontology, University of Michigan, 1109 Geddes Ave., Ann Arbor, MI 48109, USA
[b] Department of Earth and Environmental Sciences, University of Michigan, 1100 N. University Ave., Ann Arbor, MI 48109, USA
[c] Department of Earth Sciences, Denver Museum of Nature and Science, Denver, CO 80205, USA
[d] Department of Anthropology, University of Colorado, Boulder, CO 80309, USA
[e] Centre for Marine Futures, Oceans Institute, University of Western Australia, M470 35 Stirling Highway, Crawley, WA 6009, Australia
[f] Richard Gilder Graduate School, American Museum of Natural History, New York, NY 10024, USA
[g] Department of Earth and Planetary Sciences, University of California Santa Cruz, Santa Cruz, CA 95064, USA

ARTICLE INFO

Article history:
Received 19 November 2013
Available online 1 October 2014

Keywords:
American mastodon
Columbian mammoth
Pleistocene
Marine Oxygen Isotope Stage 5
Stable isotope profiles
MicroCT
Paleoclimate
Mandibular tusks

ABSTRACT

At an altitude of 2705 m in the Colorado Rockies (USA), the Ziegler Reservoir fossil site gives a rare look at a high-elevation ecosystem from the late Pleistocene (especially MIS 5) of North America. Remains of more than four mammoths and about 35 mastodons dominate the macrofossil assemblage. Mammoth remains are attributed to *Mammuthus columbi*, and mastodon remains are referred to the well-known, continent-wide *Mammut americanum*. Mastodon remains occur within and between several lake-margin slump deposits. Their deposition must therefore have occurred as events that were to some degree separate in time. We treat the mastodon assemblage in each stratigraphic unit as a source of information on environmental conditions during the lives of these individuals. Mastodon mandibular tusks are abundant at the site and represent both males and females, from calves to full-grown adults. This study presents the first attempt to use microCT, thin-section, and isotope records from mandibular tusks to reconstruct features of life-history. We recognize an up-section trend in $\delta^{18}O$ profiles toward higher values, suggestive of warmer temperatures. Throughout this sequence, mastodon growth histories show low mean sensitivities suggestive of low levels of environmental stress. This work helps frame expectations for assessing environmental pressures on terminal Pleistocene populations.

Introduction

The Ziegler Reservoir fossil site (ZRFS) just outside Snowmass Village, Colorado (USA) provides a remarkable opportunity to follow a high-altitude biota associated with an alpine lake/marsh environment through about 85,000 years of the Pleistocene (Mahan et al., 2014–in this volume; Pigati et al., 2014–in this volume). Its most numerous macroscopically identifiable remains are of proboscideans, both mammoths and mastodons. Three partial mammoth skeletons, additional mammoth molars, and disarticulated (mostly unassociated) bones and tusks representing about 35 mastodons constitute ~80% of more than 5000 macro-vertebrate specimens recovered during fall 2010 and summer 2011 excavations. In this report, we discuss both the mammoths and the mastodons found at the site, but the bones of each taxon are associated with different depositional settings. All mammoth remains were found in bog or marsh deposits near the top of the section, in what are effectively lake-center locations. In contrast, mastodon remains were mostly lower in the section, near the lake margin, in diamictic slump deposits derived from the moraine that formed the lake margin or in silty layers below and between these deposits.

For this assessment of ZRFS proboscidean material, we focus on provisional taxonomic assignment and extraction of paleobiologically and paleoclimatically relevant data from the tusk record. ZRFS mammoths present intriguing taphonomic questions, touched on below, but they are not yet thoroughly extracted from matrix and do not present a sample large enough to support comparative analysis. In contrast, the number and preservational quality of ZRFS mastodon specimens offer diverse opportunities for comparison. Our main source of insight into the lives and environments of these animals is analysis of the structure and composition of their tusks. Proboscidean tusks are ever-growing incisors composed primarily of dentin that grows through continuous apposition along a conical pulp cavity surface at the tusk's proximal end. Previous studies of proboscidean tusk growth records have featured premaxillary (upper) tusks (e.g., Fisher, 1996, 2009), and although multiple premaxillary tusks were found at the site, most required jacketing for safe removal and transport and are not yet opened, stabilized, and available for study. Mastodon mandibular (lower) tusks

* Corresponding author. Fax: +1 734 936 1380.
E-mail address: dcfisher@umich.edu (D.C. Fisher).

http://dx.doi.org/10.1016/j.yqres.2014.07.010
0033-5894/

are smaller and more compact than upper tusks and did not require jacketing. Mandibular tusks typically experience extreme attrition at their distal end, removing the record of early years of life, but they can still yield data on growth rates and compositional changes reflective of diet, nutritional status, life history, and climate during the years that remain (Fig. 1). They provide clues (if not dislodged during life) to the timing of death and conditions leading up to it. Most isolated but intact mandibular tusks probably slid out of their alveoli (near the mandibular symphysis) after death (and decomposition of their periodontal ligament). They thus provide a means of monitoring the lives of ZRFS mastodons over intervals ranging from years to decades.

Material

The first mammoth found, nicknamed "Snowy" in honor of the local village, was a young adult, represented by a large portion of a skeleton (DMNH 60676; numbers in this format are accession numbers for the Denver Museum of Nature and Science, DMNS) in Unit 15 of Pigati et al. (2014–in this volume). This specimen was damaged by bulldozer strikes before it was recognized. It also experienced significant desiccation-induced fracturing (from shrinkage stresses produced by drying).

Another mammoth, nicknamed the "Clay Mammoth" (DMNH 60704) for the clayey silt in which it was found (Unit 17, Pigati et al., 2014–in this volume), was stratigraphically above Snowy and near the lake center. The Clay Mammoth was notable for its association with a concentration of rocks (most were locally derived Maroon Sandstone) in the cobble to boulder size range. The southern margin of the assemblage was hit by a bulldozer, damaging the right tusk, but the entire assemblage constitutes less than half the skeleton. A third set of even less complete mammoth remains, "Cody's Mammoth" (Locality 87; numbers in this format are one style of field number), was encountered, also in Unit 17, as the excavation was closing. Like the Clay Mammoth, it was associated with rocks, but these were smaller and less numerous. Finally, several isolated mammoth molars were recovered as "float" or in place in Unit 17. Three of these were recovered as a single association (CCN 42–44; another style of field number).

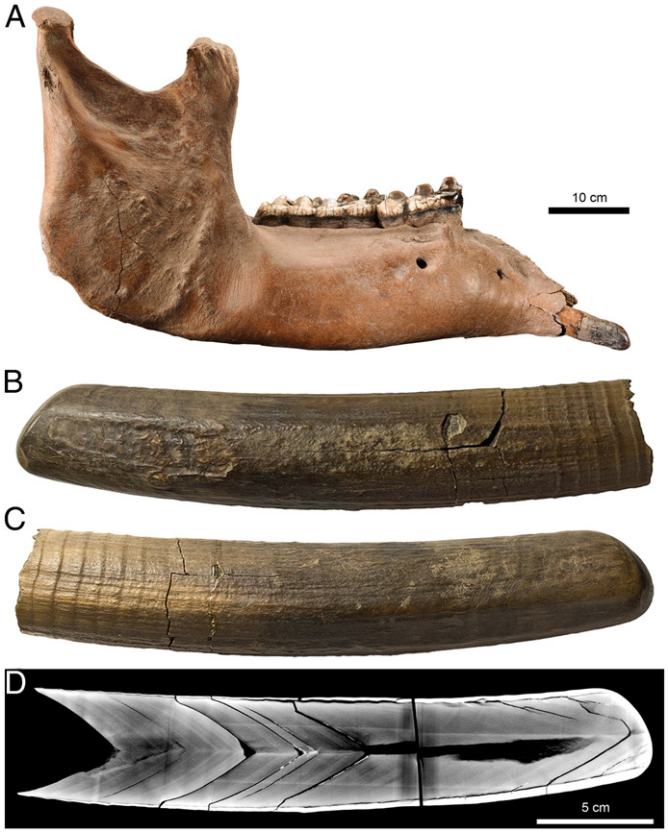

Figure 1. (A) Field no. 44.035 (DMNH) — mandible of an adult mastodon (likely female, based on molar dimensions) displaying prominent tusks. (B)–(D) Field no. 58.025 (DMNH), right mandibular tusk of an adult male (based on maximum circumference and growth increment volumes estimated from microCT scans). (B) Medial view; irregular topography on medial surface of the distal two-thirds of the tusk is antemortem interdental resorption or chemical erosion along the contact with the left mandibular tusk. Circumferential ridges ('periradicular bands') near the proximal end of the tusk are annually repeating deflections of the cementum–dentin junction. (C) Lateral view. (D) Composite microCT image along tusk axis, showing annual increments and periradicular features. Linear white features above and below (and approximately parallel to) the tusk axis are a "cylindrical artifact" produced during volume reconstruction.

ZRFS mastodon remains were found near the southeast corner of the site, along the margin of the former alpine lake. They are distributed from the clay at the base of the lake-center sequence (Unit 3, extending locally below the Basement Red Pebble unit of the lake margin) up to the Beach Silt, although the uppermost specimens do not include mandibular tusks. Our analysis of tusks for the environmental data they provide focuses on the units where mastodons are most abundant, from the Basement Silt up through the Primary Debris Flow (Pigati et al., 2014–in this volume). The ZRFS assemblage is remarkable not only in the number of specimens and individuals but also in that it represents a combination of time, region, and environment that has not been well documented for mastodons (Miller et al., 2014–in this volume). It provides an opportunity to investigate mastodon paleobiology prior to human contact and through a significant span of time.

Methods

Specimen treatment

Specimens such as the three partial mammoth skeletons were exposed (using non-metallic tools), mapped, and photographed in situ (Fig. 2A). The Clay Mammoth was also documented by three LiDAR scans. We took this step because observations made during exposure of this specimen suggested that it warranted closer study. We therefore jacketed the entire assemblage with burlap and plaster, supporting it from below with beams that were then joined into a solid framework, allowing the entire mass – bones, boulders, and surrounding sediment – to be lifted and transported to DMNS. The LiDAR scans were "insurance," in case the block's integrity was compromised during transport, but it arrived safely and has now been partly exposed, documented by total station readings on individual bones and rocks prior to their removal from the jacket, rejacketed from above, flipped, and exposed from below (Fig. 2B). Additional documentation and analysis is planned.

Isolated remains were logged into a whole-site coordinate system prior to removal. Each specimen was located by distance, azimuth, and vertical offset relative to one of a series of staked total station points around the site. Field numbers in the format "30.076" refer to the 76th specimen located in the vicinity of stake 30. Azimuth and plunge of the long axis of each element and a measure of rotational orientation about this axis (inadvertently omitted for some elements) were also taken before removal, along with photos of many bones. Bones were identified to the stratigraphic unit in which they were found; some extended across unit boundaries and were attributed to the unit containing most of their mass. Specimens from spoil piles and any removed prior to measurement were marked as "float."

Cheek teeth and mandibular tusk diameters were measured with calipers, and tusk circumferences and lengths (along the outside curve), with a flexible tape measure. Measurements (except enamel thickness) were to the nearest millimeter. Identifications of teeth were based on measures of crown size, on published descriptions (e.g., Saunders, 1977; Green and Hulbert, 2005), and on associations in intact dentaries and maxillae. Premaxillary tusks not associated with cheek teeth were identified as mammoth/mastodon from the Schreger pattern, best seen in transverse section (Trapani and Fisher,

https://doi.org/10.1016/j.yqres.2014.07.010 Published online by Cambridge University Press

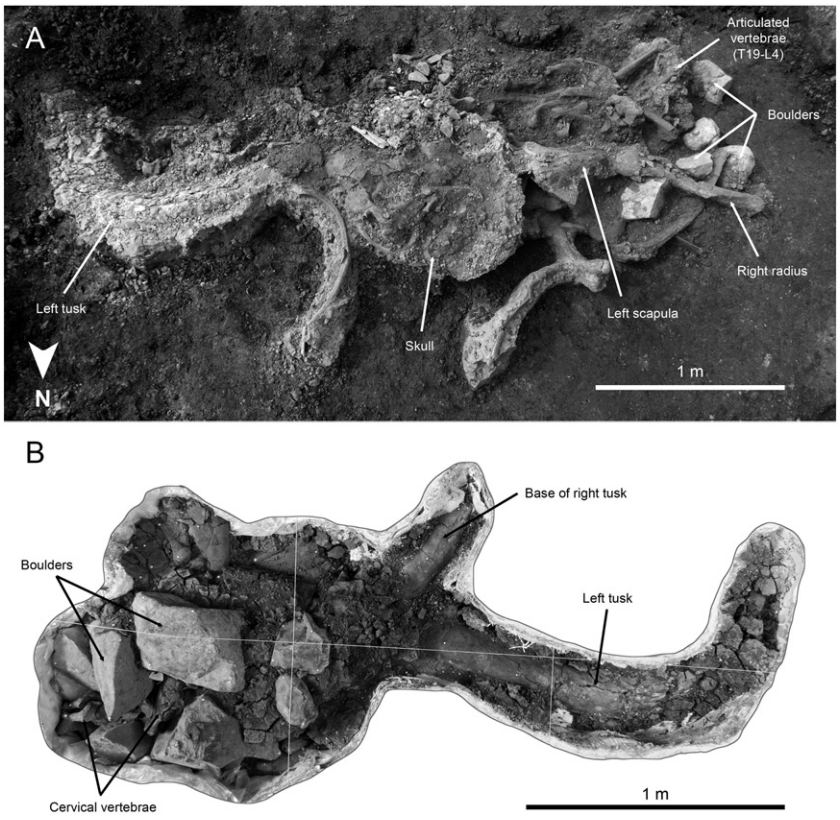

Figure 2. The Clay Mammoth assemblage (DMNH 60704). (A) In-situ field exposure, from above (north arrow at bottom-left). Numerous boulders (only some indicated) associated with the specimen are visible near the right end of the assemblage. (B) Laboratory preparation of the underside of the assemblage revealed additional boulders beneath the skull (string grid on 1-m scale).

2003). Mandibular tusks, with their shallow pulp cavities and cylindrical form, are unknown for mammoths.

To document morphology prior to any sectioning, each specimen was molded using a tin-based silicone rubber, supported by fiberglass mother molds, and then cast using pigmented polyester resin and fiberglass. Molds and first casts of each tusk will be accessioned into DMNS collections. 3D surface models of many specimens were also produced (see Supp. methods).

MicroCT analysis

Computed tomography (CT) was used to document variation in density (x-ray attenuation) of tusk dentin, revealing patterns that are interpreted below as demarcating annual increments of tusk growth. CT scans used to analyze ZRFS specimens were produced by the MicroCT Core facility in the University of Michigan School of Dentistry on a SCANCO Medical μCT100 operating at 90 kV, 78 μA, and 500 ms, yielding uniform cubic voxels 40–60 μm on a side. Some tusks had to be sectioned to fit in the chamber, scanned in multiple parts, and then reassembled virtually. In these cases we used a thin saw blade to minimize kerf loss, stopped the cut prior to completion, and fractured the last connection, allowing us to reassemble the pieces with accurate spacing. CT scans were processed in Amira 5.4.1. Volumetric measurements were acquired using Amira, but linear measurements were taken from 2D virtual slices (extracted from the CT data) that were imported into ImageJ and Adobe Photoshop. To maximize consistency between growth series in different tusks, dorsoventral slices following the long axis of the tusk were used whenever feasible (Fig. 3).

Patterns interpreted as annual variation in x-ray attenuation in most specimens consisted of a gradient from low values to high. Zones characterized in this fashion were usually followed by a relatively abrupt return to low values marking the start of the next cycle (Fig. 3). These CT features are relatively distinct but somewhat variable in clarity and always require careful inspection to determine optimal placement of boundaries. Multi-year growth trends, average growth rates, annual variability, and approximate fraction of a year that was realized at the end of life all appear to reflect meaningful variation.

Several measurement protocols were used to quantify annual increments in mandibular tusks using CT data. Data on increment thickness required a special convention because annual increments taper from the central axis of the tusk toward the cementum–dentin junction, or CDJ. Thus, no thickness measure can be exactly perpendicular to both proximal and distal increment boundaries, nor is there any point along increment boundaries at which a stable thickness value is attained. As a compromise, we located a reference point along each increment boundary, halfway between the tusk axis and the CDJ. From each such point, we constructed a line perpendicular to the increment boundary that projected toward the preceding (next-distal) increment boundary. The distance along this perpendicular from the originating boundary to the preceding boundary was used as the thickness for that increment (Supp. Fig. 1D, E). In CT data, increment boundaries are usually easier to trace midway between the axis and CDJ than along either the axis or the CDJ, so this convention could be implemented for most specimens.

Although thickness is one standard measure of increment magnitude, volumes represent an interesting alternative. With full CT scans, increment volumes can be measured directly, by digitally segmenting increments, essentially isolating and counting voxels inside the CDJ and between proximal and distal boundaries of a given annual increment. Increment volumes provide the most dimensionally comprehensive quantification of the magnitude of annual increments. However, complete segmentation is time-consuming and requires radiodensity transitions that are sharp over their entire extent. We treated some tusks in this fashion to document the relationship between increment

https://doi.org/10.1016/j.yqres.2014.07.010 Published online by Cambridge University Press

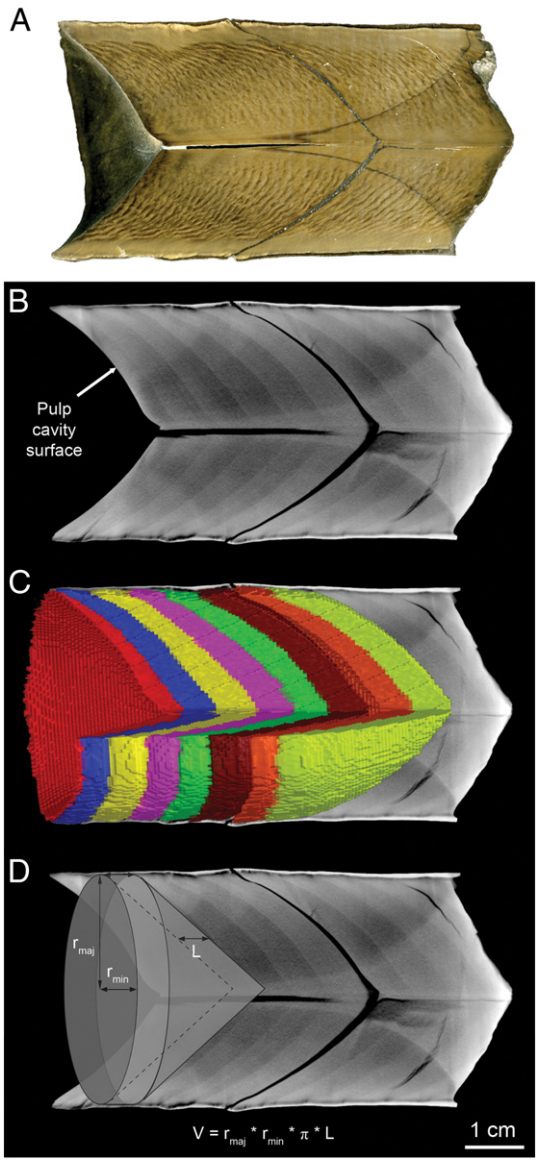

Figure 3. (A)–(D) Field no. 60.057 (DMNH). (A) Mandibular tusk cut longitudinally along axis; surface polished for isotope sampling. Schreger pattern (displayed here as tightly packed, discontinuous "tiger" stripes) obscures growth lines at this magnification. (B) Virtual 2D slice of microCT data shows radiodensity variation. Each gradual transition from dark (low radiodensity) to light (high radiodensity) producing a zonation that parallels the pulp cavity surface represents a year of growth. (C) Segmentation of microCT data enables direct volumetric measurement of annual growth increments (years distinguished by color/grayscale value). (D) Linear measurements taken from 2D projections of CT data provide a close approximation of increment volumes; *L*, increment length measured along a line half-way between axis and CDJ, r_{maj}, half the major diameter (usually dorsoventral) of the tusk at location of increment length measurement, r_{min}, half the minor diameter (usually mediolateral) of the tusk at location of increment length measurement. Estimated and measured volumes are compared in Fig. 11B.

thickness and volume, but we subsequently developed a proxy for volume that we call "estimated increment volume" (EIV).

EIV recognizes that mandibular tusks usually have an elliptical transverse cross section with a major (dorsoventral) diameter and a minor (mediolateral) diameter. EIV uses major and minor half-diameters (radii) and increment lengths (*L* in Fig. 3D, the proximodistal distance between successive originating points for thickness measures) to estimate the volume of a growth increment — approximated as the volume of a cylinder equivalent to the volume bounded by two cones separated by *L* (see also Supp. Fig. 1D, upper half of tusk). Comparisons using two tusks (60.057 and 76.085) demonstrated close agreement between EIVs and actual volumes measured from 3D CT data (Supp. Table 1).

To compare variability in growth increment series, we used a metric called mean sensitivity (MS), developed to compare variability in tree ring series (Douglass, 1920; Fritts, 1976; Laxson, 2011). MS is an index that reflects the average proportional change from one increment to the next within a series. It is calculated using the following equation, where *x* is the measure of increment magnitude (we used increment thickness), *t* indicates the position of this increment within the series, and *n* is the number of increments in the series:

$$MS_{tusk} = \frac{1}{n-1}\sum_{t=1}^{t=n-1}\left|\frac{2(x_{t+1}-x_t)}{x_{t+1}+x_t}\right|.$$

By its formulation, MS ranges between 0 and 2, with higher values representing greater disparity in consecutive increment measures. Prior to calculating mean sensitivity, the series were individually detrended by dividing each by a cubic smoothing spline with a 50% frequency response cutoff (Cook and Peters, 1981) of 20 years using the dplR package for R (Bunn, 2008), version 1.6.0. This method of removing ontogenetic trends was chosen over modeling and removing the expected trend because ages of individuals could not be determined with sufficient precision to allow alignment of growth increments by age, and normal growth trajectories are not yet well documented. When averaging MS values, we ignored series with fewer than five years.

The last year of life recorded in CT data begins with an abrupt transition in x-ray attenuation like any other year in the tusk record, but the end of this year may be different from prior year-ends, because this increment terminates when the animal dies, and that may or may not coincide with the transition in x-ray attenuation used to trace whole years in the earlier record of tusk growth. Once the typical season of transitions in x-ray attenuation has been determined, the fraction of the final year through which an animal survived gives a means of estimating season of death (SOD), but until then, we refer to this determination in more neutral terms, as "fraction (of expected growth in) final year" (FFY). FFY is a ratio of some measure observed for the final year over the corresponding measure expected for a full year. The measure of growth could be an increment thickness or length, increment area along a plane following the tusk axis, or increment volume; for most of our analyses, we used EIV. We estimated expected annual growth in three ways, distinguished in terms of how many years we used as the basis for the estimate: 1) only the last complete year, 2) the average for the last two complete years, and 3) a linear projection of the trend shown by logged values over the last five complete years.

Thin-section production and analysis

Thin-section production followed procedures used previously (Fisher, 1988); section thickness ranged from 0.25 to 0.38 mm. Slides were viewed at 40× magnification using a Leitz Laborlux Pol petrographic microscope. Small amounts of kerosene were sometimes added to a slide to enhance light transmission and clarify growth increments. Digital photographs taken with a camera mounted on the microscope were analyzed using an ImageJ measurement utility (IncMeas 1.3c; Rountrey, 2009).

Proboscidean tusk dentin contains three scales of growth features, two of which require thin-sections for precise analysis. First-order features are often visible without magnification and represent annual growth increments. Third-order features represent daily dentin apposition and are sometimes seen in thin-sections under magnification, but are rarely clear enough to permit serial growth measurements. Second-order features, also best seen in thin-section, are strongly developed third-order features that occur with fairly consistent periodicity. The periodicity of second-order features can differ between taxa and dental elements. In mastodon premaxillary tusks, second-order features have a periodicity of approximately two weeks (Fisher, 1987, 1996), but periodicity of these features has not been analyzed previously in mastodon mandibular tusks. Growth analyses of thin-section data focus on variations in thickness of second-order increments.

https://doi.org/10.1016/j.yqres.2014.07.010 Published online by Cambridge University Press

Analysis of stable isotope profiles

After 3D digitizing, molding, and casting, mandibular tusks being prepared for isotope sampling were sectioned longitudinally parallel to, but about 2 mm to one side of the axis. The larger half, including the axis, was then polished in preparation for sampling (usually without removing a 5-mm slab). We then milled samples of dentin 1–2 mm deep across this longitudinal surface without significant time-averaging (see Supp. methods).

Second-order growth lines visible in images of the specimen surface (acquired by flatbed scanner and digitally enhanced to accentuate features) and traceable under magnification guided design of a series of mill-paths sampling dentin formed during consecutive, non-overlapping intervals of time. Where growth lines were difficult to follow, macroscopically visible first-order features and boundaries transferred from microCT results also assisted in sample planning. For the first tusks studied (two adult premaxillary tusks and two mandibular tusks), sample plans were mapped on a magnified image of the polished surface, printed at actual size on acetate sheets, and then transferred to the tusk, followed by hand-milling under a stereomicroscope. For subsequent studies, we increased accuracy and precision (critical for the relatively thin years of mandibular tusks) by programming mill-paths (e.g., Supp. Fig. 2) into the computer-controlled Merchantek MicroMill in the University of Michigan Stable Isotope Lab (UMSIL).

Samples were milled using either a 0.5-mm round carbide burr or a 1-mm diamond cylindrical bit. To acquire samples narrower than one bit-width, milling proceeded via shallow passes initiated from the open pulp cavity and progressed inward toward earlier growth markers.

Analyses of structural carbonate in dentin were performed on powder samples pretreated using the procedure documented by Rountrey (2009), and collagen preparation methods were based on those outlined by Rountrey et al. (2007) (see also Supp. methods). Collagen and carbonate samples reported here correspond directly, with each collagen sample having a carbonate sample complement that was milled from the same growth interval. Results for carbonate and collagen analyses are reported in delta notation relative to VSMOW ($\delta^{18}O$), VPDB ($\delta^{13}C$), and air-N_2 ($\delta^{15}N$).

Results

Taxonomic overview

Most proboscidean taxonomic discrimination focuses on the morphology of third molars (Maglio, 1973; these are the largest teeth, with the longest functional life and the greatest likelihood of recovery). A partial right lower third molar (m3; DMNH 60704.008) with 16 lophs, 9 of which are exposed on the occlusal surface, was dislodged by the bulldozer that grazed the southern edge of the Clay Mammoth assemblage (Fig. 4, Supp. Fig. 3). Two molar fragments found with Cody's Mammoth represent a left m3 (Loc. 87–44; differences in stage of tooth wear and duplication of seventh cervical vertebrae and right first ribs between these two occurrences preclude interpreting them as a single individual) similar to that of the Clay Mammoth (Table 1). Three first and second molars were recovered for Snowy (DMNH 60676, Table 1), a younger individual, and another three first and second molars (CCN 42–44, Table 1) were recovered in an association separate from the three partial skeletal assemblages.

Molar form for the Clay Mammoth and Cody's Mammoth, and for the isolated teeth (not treated here, but to be described elsewhere) is entirely consistent with *Mammuthus columbi* (Falconer, 1857), for which comparative data are given in Saunders (1970), Graham (1986), and Agenbroad (1994). Snowy's molars are likewise readily accommodated within this taxon, although her enamel is thinner than expected. The only observations that complicate this simple picture are the relatively narrow crowns, the high lamellar frequencies, and the relatively thin enamel of CCN 42–44, traits that are at least suggestive of *M. primigenius*. Plate number for these molars is still within expected range for *M. columbi*, but this mosaic of traits raises the possibility that we are seeing morphological evidence for introgression between *M. columbi* and *M. primigenius*, as has been proposed on the basis of mtDNA evidence (Enk et al., 2011).

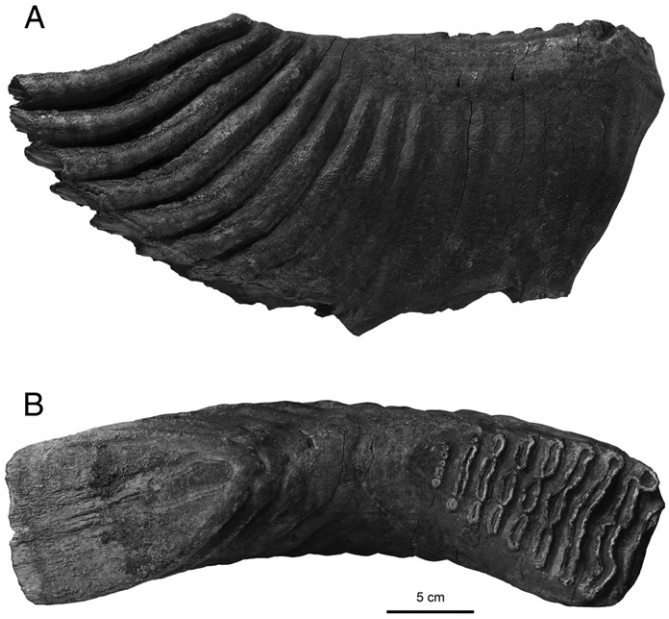

Figure 4. (A) Buccal and (B) occlusal views of lower right third molar (DMNH 60704.008) from the Clay Mammoth.

Measurements of a subset of cheek teeth of ZRFS mastodons are presented in Supplementary Tables 2 and 3, and natural logarithms of molar lengths and widths are plotted over comparable data for *Mammut americanum* from the Great Lakes region in Supplementary Figure 4. We could of course use larger sample sizes on both sides of this comparison (and more are available for a more comprehensive analysis), but ZRFS mastodons shown here present no clear metric differences from other well-documented North American occurrences of the genus. Likewise, finer details of tooth form (Supp. Fig. 5) correspond closely to material attributed to the American mastodon (e.g., Saunders, 1977). On this basis, we provisionally refer ZRFS mastodons to *M. americanum* (Kerr, 1792).

Table 1
Molar measurements for ZRFS mammoths.

Specimen	Tooth	L (cm)	P	P_{occ}	W (cm)	H (cm)	LF	E (mm)
Clay Mammoth								
60704.008	Rm3	>33.4	16+	9	8.7^{3}	15.9	7.0	2.0
Cody's Mamm.								
Loc. 87-44	Lm3	>29.5	15+	1	9.5^{2}	17.5	6.0	2.2
Snowy								
60676.001	Lm1	16.4	11	11	7.1^{6}	in jaw	7.0	1.5
60676.194	LM1	17.0	11	11	7.8^{5}	in max.	7.0	1.5
60676.007	RM1	16.5	11	11	8.0^{6}	in max.	7.5	2.0
Assoc. molars								
CCN 44	Lm1	12.2e	10	10	6.0^{5}	>7.0	8.5	2.0
CCN 42	Rm2	>16.1	11+	2	6.5^{2}	13.0	9.0	1.5
CCN 43	LM2	>17.8	14+	1	5.1^{3}	14.0	8.5	1.5

Abbreviations: Tooth descriptors, L, R (left, right), M (upper molars), m (lower molars); L (cm), tooth length; P, number of plates (lophs); P_{occ}, number of plates exposed on occlusal surface; W (cm), maximum tooth width (superscript indicates plate at which this is attained, from front of tooth); H (cm), crown height; LF, lamellar frequency (number of plates per decimeter of tooth length); E (mm), enamel thickness; >, incompleteness of tooth (plates missing distally or extensive occlusal attrition), such that value recorded underrepresents original dimension; +, plates missing distally; in jaw, in max., tooth is retained in the mandible or maxilla, such that crown height is inaccessible.

https://doi.org/10.1016/j.yqres.2014.07.010 Published online by Cambridge University Press

Nonetheless, we have noticed differences between ZRFS mastodons and populations from elsewhere in North America. For example, premaxillary tusks of male mastodons in the Great Lakes region show a helical component to their curvature that is notable, but visually subordinate to the arcuate curvature conspicuous in lateral view. In contrast, the best preserved ZRFS mastodon premaxillary tusk shows a much more pronounced helical curvature (Supp. Fig. 6). In addition, the surface of Great Lakes region mastodon tusks is relatively smooth, with only subtle longitudinal ridges and grooves, whereas ZRFS mastodon premaxillary tusks, both male and female, show a pattern of longitudinal fluting expressed most strongly at the cementum–dentin junction (although it carries through to the external surface of the cementum). This pattern consists of centimeter-scale grooves separated by narrow ridges that twist (dextrally on left tusks, in concert with their overall helical form; sinistrally on right tusks) around the structural axis of the tusk. These differences and others, such as the common occurrence of mandibular tusks in ZRFS female mastodons, as well as males (see below) have raised the possibility that ZRFS mastodons could represent a new species. However, many specimens remain unprepared, and quantitative morphologic studies have barely begun. In view of the abundance of material that should be considered, recognition of a new species at this time would be premature.

Demography

The Clay Mammoth molar examined above suggests a Laws' Age Class of XX–XXII, equivalent to an African elephant age of 34–39 yr (Laws, 1966). Tusk circumference and length of this individual (48 cm, 195 cm — estimated) indicate a male, based on sexual size dimorphism, which is especially clear in tusks (Fisher, 2008; Smith and Fisher, 2011). Patterns of epiphysis fusion are consistent with an adult male almost, but not yet, fully grown (Haynes, 1991). Cody's Mammoth suggests a Laws' Age Class of XVIII (ca. 30 ± 2 yr) but currently offers no clear evidence of sex. Snowy suggests a Laws' Age Class of XII (ca. 18 ± 1 yr), and with a tusk circumference and length of ca. 35.9 and 60 cm, must be a sub-adult female.

Mastodon dentitions can also be age-ranked using Laws' Age Classes, as shown by Saunders (1977), though stages of eruption and wear in mastodons do not precisely correspond to those seen in elephants and mammoths, and implied ages are even less likely to match elephant ages (Fisher, 1996). Figure 5 is a first attempt to census ZRFS mastodons, based on elements of the mandibular dentition. Our general approach was to use Laws' Age Class (where available), stratigraphic provenience, and left–right identity to attempt to rule out double-counting of individuals. For isolated mandibular tusks (offering no basis for assigning Laws' Age Class), we supplement stratigraphic provenience and left–right identity by checking for matching overall lateral profile, maximum circumference, and lateral profile of dorsal and ventral wear facets at the distal ends of tusks, all of which show strong similarities in left–right pairs present within the collection (e.g., field no. 44.035). Similar comparisons make it unlikely that any of the isolated tusks come from empty alveoli in mandibles with lower dentitions. The smallest tusks are clearly deciduous (with closing pulp cavities, and some with initial stages of proximal resorption). Some of these could be premaxillary rather than mandibular, but this would not affect the count by more than a few. Some other mandibular specimens are unprepared, and many isolated cheek teeth have not yet been assigned to individuals, so the ~35 specimens in this plot (39 are shown, but we conservatively discount a few) are probably an undercount for the whole site (broken tusk tips and expectorated cheek teeth were excluded because they could represent antemortem events).

Attribution of sex to the larger mandibular tusks is based on the evident size-dimorphism in tusks. Scanning the bivariate portion of Figure 5, for specimens with a Laws' Age Class > XV (a stage at which an African elephant would be 24 ± 2 yr, and sexual dimorphism would already be well developed), there is a separation in maximum

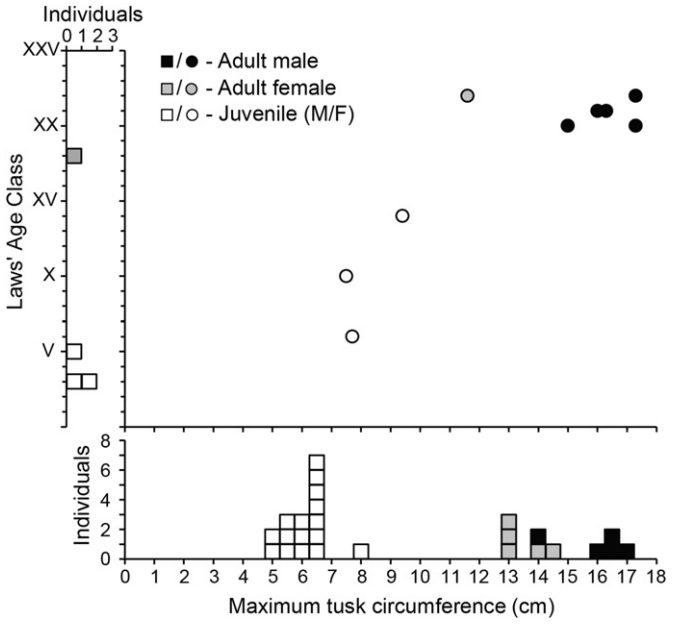

Figure 5. Partial census of ZRFS mastodons using mandibular tusk circumferences and stage of cheek tooth eruption and wear to determine relative ages of individuals. Main area of figure is a bivariate plot of Laws' Age Class determinations (Laws, 1966) vs. maximum circumference of mandibular tusks for specimens for which both can be assessed. At left is a histogram of additional specimens (mandibles without tusks) for which maximum tusk circumference cannot be assessed. Below is a histogram of additional specimens (isolated tusks) for which no Laws' Age Class is available (maximum tusk circumference rounded to nearest 0.5 mm).

tusk circumference between one specimen identified as an adult female and five identified as adult males. Projecting down to the histogram below the bivariate plot, three isolated mandibular tusks with circumferences of about 13 cm are identified as adult females, and four tusks with circumferences of 16–17 cm are identified as adult males. The three tusks in between, with circumferences of 14–14.5 cm were identified on the basis of EIV trends discussed below. In short, we see here a pattern that parallels the well-documented dimorphism in premaxillary tusks (Smith and Fisher, 2011).

Taphonomy

Most taphonomic issues beyond season of death will be treated in subsequent papers. However, a few taphonomic observations emerged in the course of research performed to meet the explicit goals of this paper and are of general interest. Among these, several features of the Clay Mammoth are notable. The Clay Mammoth includes some articulated remains (e.g., a series of thoracic and lumbar vertebrae), but most bones are disarticulated, although in some cases in approximate relative anatomical positions. Some of the assemblage remains unexcavated, so the inventory of bones is incomplete. Parts of both fore and hind limbs are present, as well as parts of the axial skeleton, and yet less than half the skeleton is present. During initial excavation, we encountered a small rib fragment completely surrounded by peat and with transversely oriented marks that we initially considered as possible cutmarks. At the time, we knew little about the age of the specimen and decided to err on the side of caution in considering explanations for this assemblage. The most unusual aspect of the assemblage was the suite of boulders, which were both above and below bones; no simple statement of precedence applies consistently to these categories of material. Subsequent analysis of these boulders has identified several refits on non-adjacent fragments, requiring a more complex history than was evident at first. During excavation of the entire expanse of units 16 and 17, few if any other rocks of comparable size were encountered, and none in this type of concentration. The only

https://doi.org/10.1016/j.yqres.2014.07.010 Published online by Cambridge University Press

hint of a similar pattern is the smaller set of smaller rocks found with Cody's mammoth.

MicroCT analysis

MicroCT scans of ZRFS proboscidean tusks show variability in x-ray attenuation of dentin paralleling growth increments, indicating that changes in dentin radiodensity occurred during growth. As described under Methods, the typical pattern of variation is a gradient from lower to higher values (in the direction of apposition), followed by a relatively abrupt drop to lower values initiating the next cycle. This high-to-low drop is the only density-feature well-defined enough in most specimens to use for serial measurements of radiodensity increments. In addition to the repetition of this pattern, its spatial scale is relatively constant within and between mandibular tusks.

Recognizing increments as annual does not identify the season of any given part of the cycle, but striving toward this goal, we have followed the high-to-low density drop along second-order increments, in thin section and on thick, polished sections, tracing it to the CDJ. In tusks where the CDJ shows a series of topographic features known as periradicular bands (common in adult males, as in Figs. 1B–D, and variable in expression, from broad undulations to quite discrete topographic anomalies), density drops are closely aligned with periradicular bands. This association will figure in our discussion of the seasonal significance of radiodensity features.

MicroCT records for six small deciduous tusks (17.1/60696; 44.146; 68.032; 68.050; 71.092; 77.099) contain a brief density decrease that can be traced from the crown into the root. This density anomaly presents as a dark line on polished sections in reflected light (Fig. 6). We interpret it as a neonatal line, marking the time of birth. Most ZRFS tusks in this size range lack clear annual radiodensity features, either because these animals were too young to show more than part of a year or because, as nursing juveniles, they were buffered from seasonal variability.

Thin-section analysis

To explore the relationship between radiodensity variation and rate of dentin apposition, we examined transverse thin-sections of the final years of growth in two premaxillary tusks of ZRFS mastodons, one adult male and one adult female (based on tusk diameters; Loc. 8 and 70.018, respectively). Figure 7 shows results for the male, where drops in x-ray attenuation are preceded by thin second-order increments (slow growth) and followed by thicker second-order increments (more rapid apposition), supporting the hypothesis that density drops are associated with winter–spring boundaries. Results for the female premaxillary tusk were similar. Thin-sections from two mandibular tusks (58.360, 45.015) were more difficult to analyze, with less distinct second-order features.

Isotope analyses

$\delta^{18}O_{[carbonate]}$

Oxygen isotope values from serial sampling of ZRFS mastodon tusks show remarkable consistency between specimens (all isotope values are reported in Supp. Table 4). Most were sampled over a succession of annual increments that would have formed over an interval of 3–4 years. Profiles generally contain one oscillation per year, with some smaller-scale fluctuations and an amplitude of about 3‰ (Figs. 7C, 8, 9). Peak values are associated with the low-density dentin that we provisionally designated as spring in our interpretation of CT data. The annual oscillations conform well to expectation, but peaks occur earlier in the year than in Great Lakes region specimens (Koch et al. 1989). Annual amplitudes are lower than we often see (Koch et al. 1989) but comparable to other cases (Fisher and Fox, 2003); we expect both hydrological and physiological processes exert a damping effect on annual amplitude.

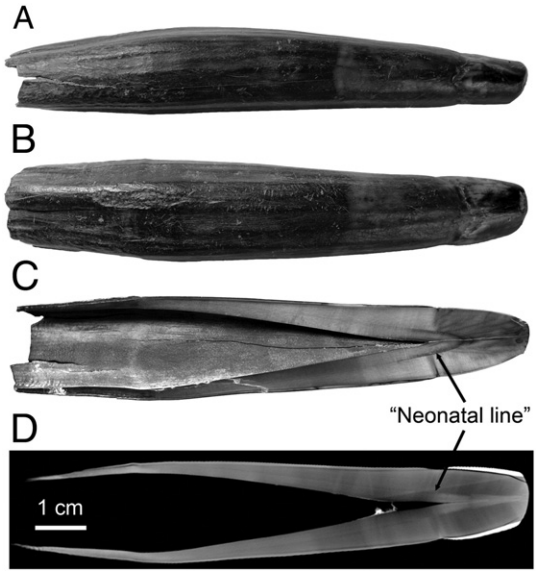

Figure 6. Field no. 68.050 (DMNH). (A) and (B) Two exterior views (orthogonal to each other but with uncertain anatomical orientation) of a deciduous mastodon tusk. Enamel crown is intact. Color/grayscale boundary on cementum surface at gingival margin (approximately 1/3 distance from distal end) and smoothly worn crown indicate tusk had erupted. (C) Tusk cut longitudinally along axis (polished in preparation for isotope sampling; some enamel spalled during polishing) displays a deep pulp cavity and distinct feature recognized as a neonatal line. (D) Virtual longitudinal slice through microCT data (enamel is bright white) displays a radiodensity manifestation of the neonatal line. This feature is present in approximately the same location in all ZRFS deciduous tusks analyzed.

Average $\delta^{18}O$ values for ZRFS tusks generally increase up-section (i.e., tusks from younger strata tend to have more enriched oxygen isotope ratios). This is probably not a diagenetic effect because the tusks in question come from a similar set of lithologies, and few show unexpected shifts in isotopic values near specimen surfaces, where exposure to pore fluids would have been greatest. We suspect that the up-section increase in oxygen values represents regional climate change during the period of mastodon occupation.

Fine-scale sampling in two of the six deciduous tusks with neonatal lines (17.1/60696; 68.050) yields $\delta^{18}O$ records that exhibit an oscillatory pattern consistent with data from other tusks. This is expected, as both fetal and newborn values should track the mother's oxygen values. Because these tusks have no clear annual features, the temporal scale of this variation is currently unclear. However, using apparent second-order features visible in each record and comparative growth rate data from other proboscidean deciduous tusks, we should be able to compare timing of the neonatal line to the seasonal oxygen pattern to deduce the season of birth.

$\delta^{13}C_{[carbonate]}$

Carbon isotope results from structural carbonate in samples of dentin powder for ZRFS tusks range from −3.16 to +4.27‰ (individual tusk averages). The highest of these values are unexpected for any mammalian herbivore, even committed C_4 feeders (Koch et al., 1994). This, in combination with the high level of variation among individuals, is suggestive of diagenetic alteration of dentin carbonate. Dentin carbonate is known to be more susceptible to alteration than enamel carbonate — Koch et al. (1997) observed high variation and many elevated $\delta^{13}C$ values for dentin carbonate of Great Lakes region mastodons (range −13.1 to +0.4‰), while enamel carbonate and collagen carbonate showed consistent values expected of C_3 browsers and much less variability in each (standard deviations of 1.0 and 1.3‰, respectively).

https://doi.org/10.1016/j.yqres.2014.07.010 Published online by Cambridge University Press

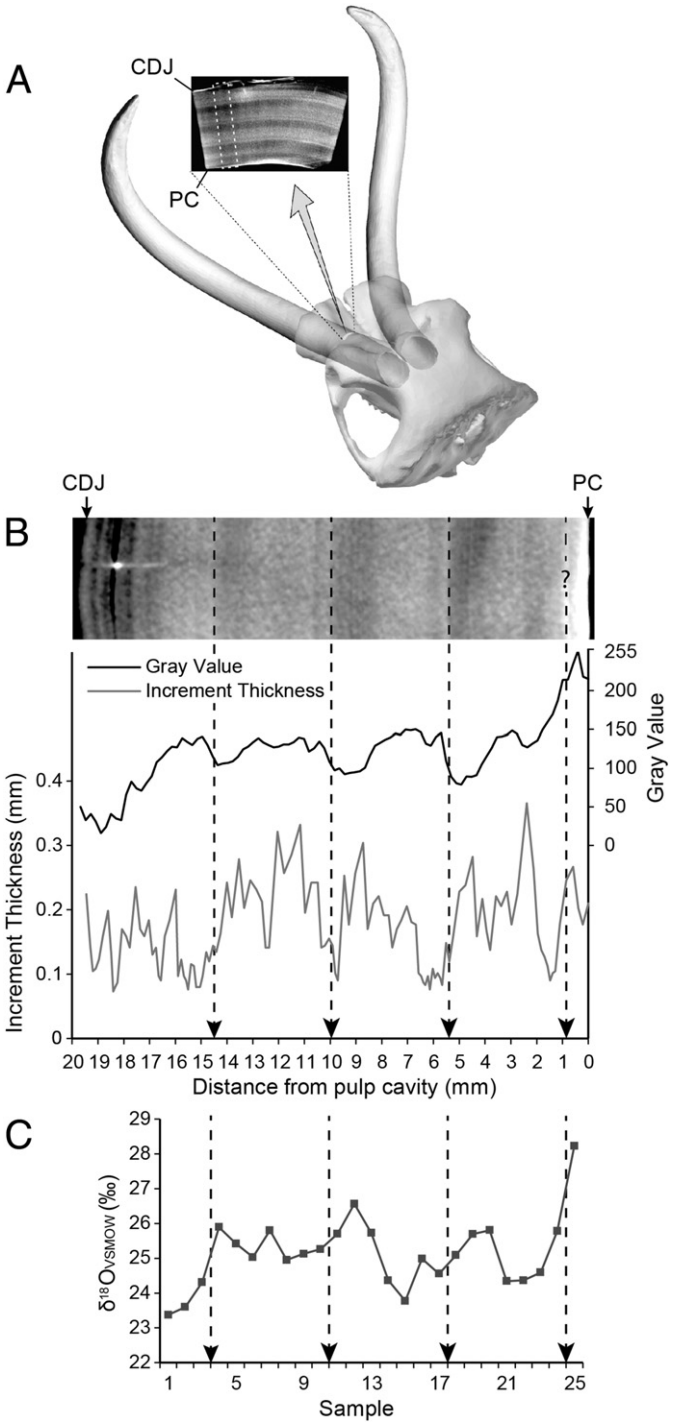

Figure 7. Locality 8 (DMNH). (A) Digital skull and tusks at top show source of tusk sample (microCT inset; white dashed lines frame cropped CT image (CDJ to pulp cavity, PC) enlarged below). (B) Extracted region of interest in A, from CDJ at left to PC at right. Below this (y-axis label on right) is a plot of luminance (gray values measured on a scale of 0 [black, lower density] to 255 [white, higher density] measured in ImageJ) along a transect from CDJ to PC and a graph of second-order increment thicknesses along the same transect, from a thin section of the same dentin sequence (x-axis records distance from pulp cavity). Black dashed lines mark drops in radiodensity. (C) Oxygen isotope values from the same specimen cover the last three-plus years of life. Second-order profile and oxygen isotope results suggest a final winter–spring boundary not visible in CT data.

Many ZRFS tusk individual time series showed little variation, and some had more enriched $\delta^{13}C$ carbonate values near the exposed pulp cavity surface, additional evidence of diagenetic alteration.

To further evaluate this finding, we isolated a bulk sample of enamel from 68.050 (Fig. 6), a deciduous tusk with enamel present distally.

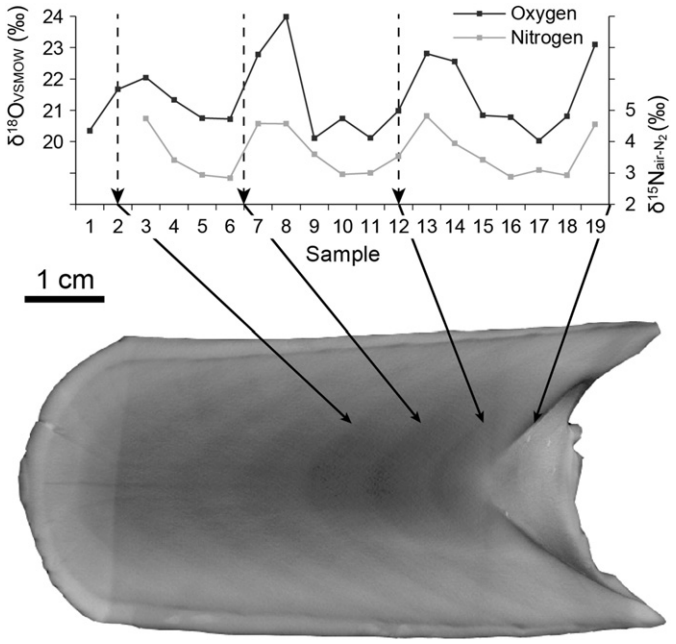

Figure 8. Oxygen and nitrogen isotope data for sub-adult male mastodon mandibular tusk (Field no. 58.360). Vertical dashed lines indicate locations of annual CT features in image below graph (abrupt transition from high to low density). Nitrogen record is in phase with oxygen profile.

Given its coarser crystal size and lower permeability, we would expect this tissue to be less susceptible to alteration, and indeed, the mean $\delta^{13}C$ (three analyses) of its structural carbonate was −7.79‰ (s.d. = 0.11; Supp. Table 3).

$\delta^{15}N_{[collagen]}$

Collagen samples for two mandibular tusks (45.015; 58.360) exhibit clear and consistent nitrogen isotope patterns that correlate closely with CT density features (Fig. 8). One way of assessing collagen preservation is to be suspect of samples with carbon–nitrogen molar ratios below 2.9 or above 3.6, a range determined empirically from measurements of modern bone (DeNiro, 1985). One tusk (45.015) has C/N ratios between 3.25 and 3.46 — high, but within acceptable values. C/N for samples from 58.360 falls mostly between 3.50 and 3.63 with two higher values up to 3.89. If preservation is questionable here and not in 45.015, degradation does not appear to have affected the nitrogen values, because $\delta^{15}N$ series from both tusks display similar patterns with similar ranges (58.360 values in Fig. 8).

Nitrogen isotope series for both mandibular tusks sampled exhibit annually repeated oscillations with amplitudes of about 2‰. Just as in carbonate oxygen results, peak values correspond to samples from the low-density phase of annual CT cycles.

Collagen samples from two mastodon premaxillary tusks (Loc. 8 and 70.018) included samples with C/N ratios that were farther outside the accepted range. In these tusks, samples frequently broke up during demineralization and remaining collagen was visibly degraded — sometimes leading to complete sample loss. Serial samples for Loc. 8 were not analyzed, and with multiple lost samples in 70.018, it is unclear whether the $\delta^{15}N$ pattern is similar to those observed in mandibular tusks, but values fall within the same 2‰ range.

$\delta^{13}O_{[collagen]}$

Carbon isotope ratios in all collagen samples matched expectations for C_3 browsers and displayed no cues suggesting alteration. They are therefore likely more reliable than values from dentin carbonate powder samples but are not useful for seasonal determination because they lack any clear pattern of intra-annual variation (Supplementary Table 4: 45.015, 58.360, 70.018).

https://doi.org/10.1016/j.yqres.2014.07.010 Published online by Cambridge University Press

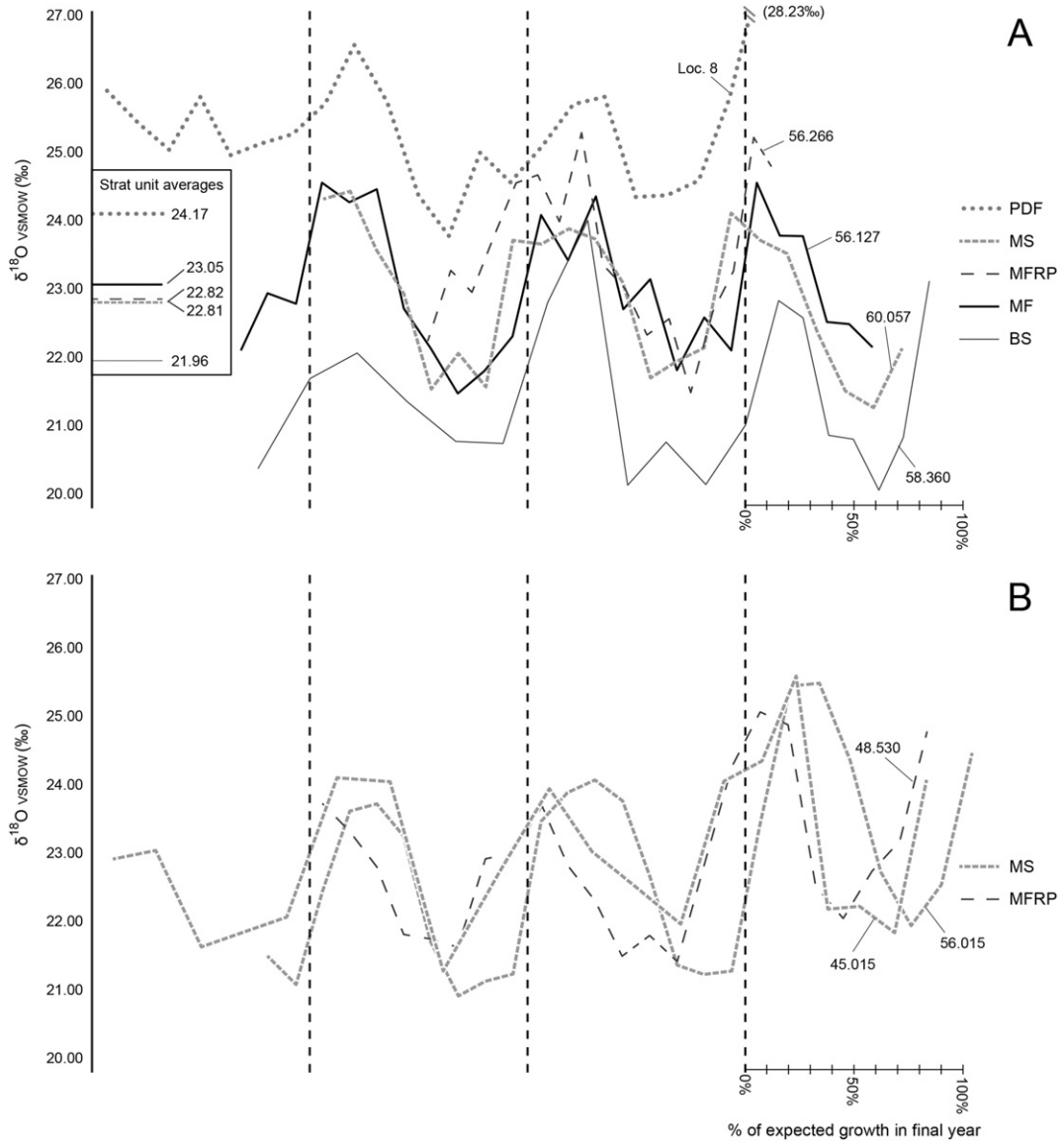

Figure 9. (A) Comparison of multi-year oxygen isotope series for mastodon tusks from different stratigraphic units. Vertical lines represent locations of annual CT features (abrupt transition from high to low density); fraction of final year is plotted as a percentage of expected growth for a complete year (see Fig. 10). Because different tusks and different years within the same tusk may have different numbers of samples per year, sample intervals are spaced variably along the x-axis and aligned to annual CT features. Tusk isotope records from the oldest unit sampled (BS, Basement Silt) produced average $\delta^{18}O$ values ~2.1‰ lower than those of specimens obtained from the highest unit sampled (PDF, Primary Debris Flow). Tusks from intermediate units (MF, Main Floor; MFRP, Main Floor Red Pebble; MS, Main Silt) consistently show $\delta^{18}O$ values between the two extremes. Horizontal lines mark average $\delta^{18}O$ values over all specimens sampled from each unit (BS — 3 spec., MF — 1 spec., MFRP — 4 spec., MS — 3 spec., PDF — 3 spec.). (B) Two mandibular tusks from Main Silt (MS) and one from the subjacent (and potentially genetically related) Main Floor Red Pebble (MFRP) have similar seasons of death and similar $\delta^{18}O$ series.

Fraction (of expected growth in) final year

CT scans of dentin from the anterior root of the right m3 (DMNH 60704.008) of the Clay Mammoth showed density variation indicative of annual increments for the final 3–4 years of life. This series was not long enough to establish trends or meaningful variation but did allow us to establish FFY (using linear measurements, not EIVs), the fraction of expected growth in the final year. The Clay Mammoth died about 60% of the way into its final year (Fig. 10). We leave the seasonal interpretation of this fraction to the Discussion section. Scans of blocks cut from two adult mastodon premaxillary tusks (Loc. 8 and 70.018) also did not contain enough information to evaluate variation in growth but again provided FFY determinations (based on linear measurements, not EIVs; Fig. 10).

Scans of six deciduous tusks (17.1/60696; 44.146; 68.032; 68.050; 71.092; 77.099) contain only one distinct feature, a brief density drop identified above as a neonatal line. These are different from all other radiodensity features observed in this study, but without annual increments, the CT record yielded no FFY. However, one juvenile (but permanent) premaxillary tusk (56.266) contained parts of three annual density cycles but no neonatal line, despite being essentially complete, implying that it initiated formation following birth. Like other tusks with short annual series, this scan was useful *only* for FFY (based on thicknesses; Fig. 10).

Twenty-one mastodon permanent mandibular tusks containing multiple years were analyzed by microCT (Table 2). As noted above, these are interpreted as derived from different individuals (with the exception of one pair: 49.594 and 49.595), and they span five stratigraphic units (Basement Silt through Primary Debris Flow). Based on circumference and growth measurements, they appear to include nine adult males, seven adult females, two adolescent males, and two sexually indeterminate juveniles (Fig. 11). EIVs (estimated increment volumes)

https://doi.org/10.1016/j.yqres.2014.07.010 Published online by Cambridge University Press

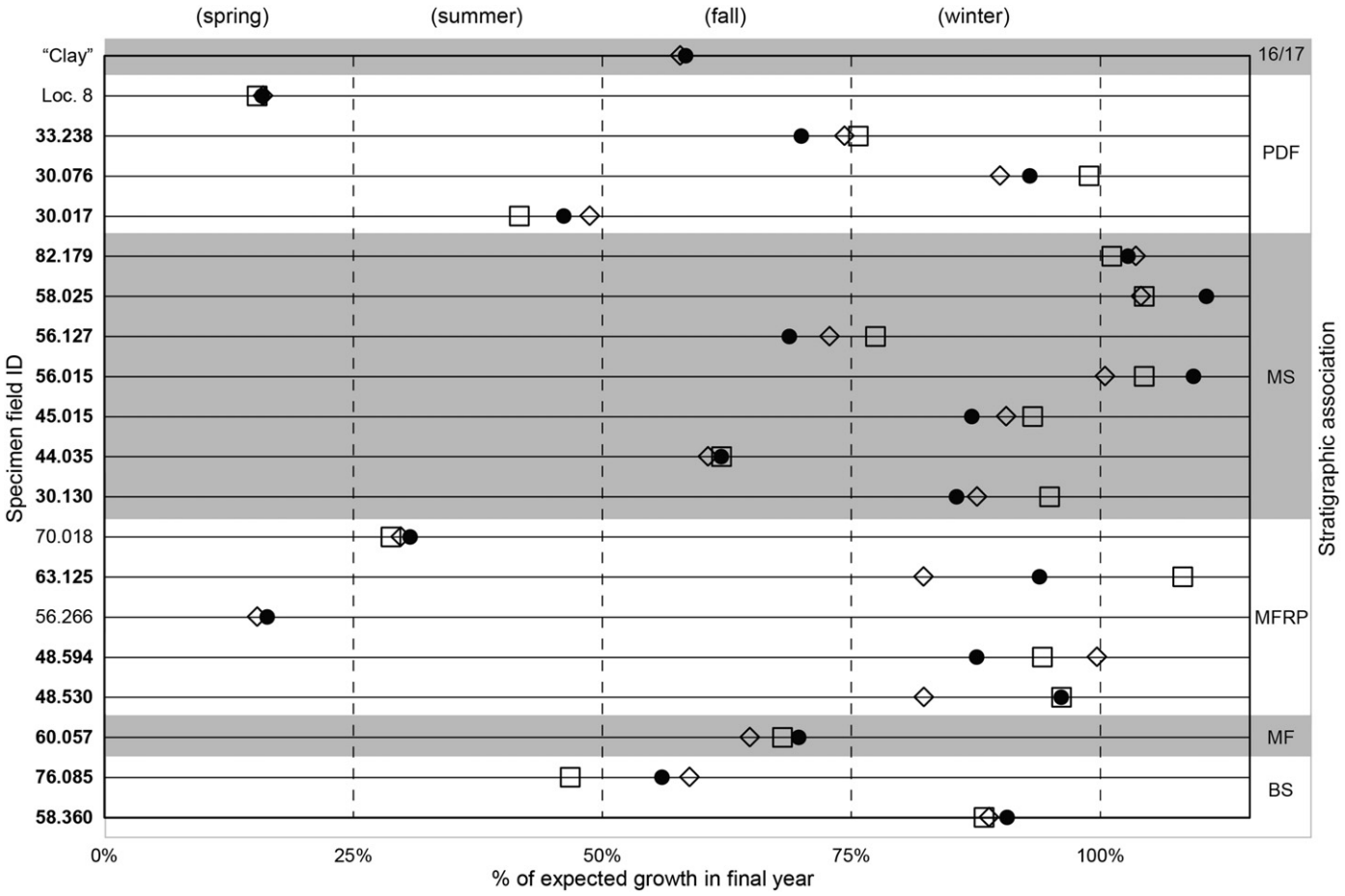

Figure 10. Fraction [of expected growth in] final year (FFY) for ZRFS proboscideans, grouped by association with stratigraphic units in Pigati et al. (2014–in this volume): [Lake-margin] BS, Basement Silt; MF, Main Floor; MFRP, Main Floor Red Pebble; MS, Main Silt; PDF, Primary Debris Flow; [Lake-center] 16/17, boundary between units 16 (peat) and 17 (clayey silt). Units arranged in succession with youngest at top; order of specimens within units is by field number. Specimen numbers for mandibular tusks are in bold. Each estimate expresses the final increment volume as a percentage of annual increment volume expected for a complete year. For solid circles, expected volume = EIV for the last complete year; for open diamonds, expected volume = average EIV for the last two complete years; for open squares, expected volume is projected from a 5-yr linear trend (except for 56.127 and Loc 8 in which only three previous years are available) of logged EIVs. Data for Loc 8, Clay, 44.035, 70.018, and 56.266 are based on linear measurements rather than EIVs. Symbols beyond 100% (e.g., 56.015) reflect either an uncharacteristically productive year or failure to recognize an obscure final feature. Numerous individuals from the Main Floor Red Pebble and Main Silt display a season of death near the end of an annual CT density cycle. Provisional seasonal designations (based on evidence presented in the Discussion) for each quarter of an expected year's growth are listed in parentheses along the top of the graph.

were calculated for all these tusks, and all display breakage and/or wear at their tips, indicating that the record of the earliest years of life has been lost. Increment series for adult tusks suggest a bimodal distribution, with most increments plotting either in the upper or lower range of logEIV values indicated on the right border of Figure 11. In addition, one adult from the Main Silt (MS) has proximal increments within the female range but a circumference (on a part of the tusk not scanned) that suggests it is a male. Its declining EIVs suggest it may be senescent.

Some other specimens display a decreasing EIV trend over the final years of growth. Most of these tusks are also decreasing in circumference as death approaches, and they have shallow pulp cavities, characteristics typical of older individuals. However, a few exhibit decreasing increment trends with increasing circumferences and relatively deep pulp cavities. This could indicate that slowed increment growth precedes the reduction in tusk circumference that occurs in older individuals.

FFY evaluations were impossible for five tusks with missing proximal ends. For the remaining specimens, FFYs for ten tusks fall near the completion of the final cycle (Fig. 10). One tusk's final increment measures 111% of expected volume, meaning either that the final year was unusually productive or that the final increment boundary is unclear, and growth actually persisted into the beginning of a subsequent, undetected cycle. Likewise, some that appear to have stopped short of a full year, could have been growing more slowly at the end of life and completed more of their final year than is evident by this calculation.

One additional mandibular tusk (44.035) was found within the alveolus of an adult mandible (probably female) and was measured for EIVs through most of its length, up to its last three years, at which point root bifurcation complicated calculation of EIV. FFY was estimated for this tusk using increment length measurements alone.

Comparing EIVs among individuals and stratigraphic units does not reveal any trends in growth rates correlated with time (Fig. 11), and growth variability, quantified as mean sensitivity, also shows little change through time. Two adult and one sub-adult record from the lowest layer sampled (Basement Silt) average 0.07. The average of three tusks from the uppermost layer sampled (Primary Debris Flow) is 0.08, and 12 tusks from intermediate layers (Main Floor, Main Floor Red Pebble, and Main Silt) have an average value of 0.08.

Discussion

New sites frequently raise taxonomic issues, and the ZRFS mammoths are no exception. We were interested in seeing whether there

https://doi.org/10.1016/j.yqres.2014.07.010 Published online by Cambridge University Press

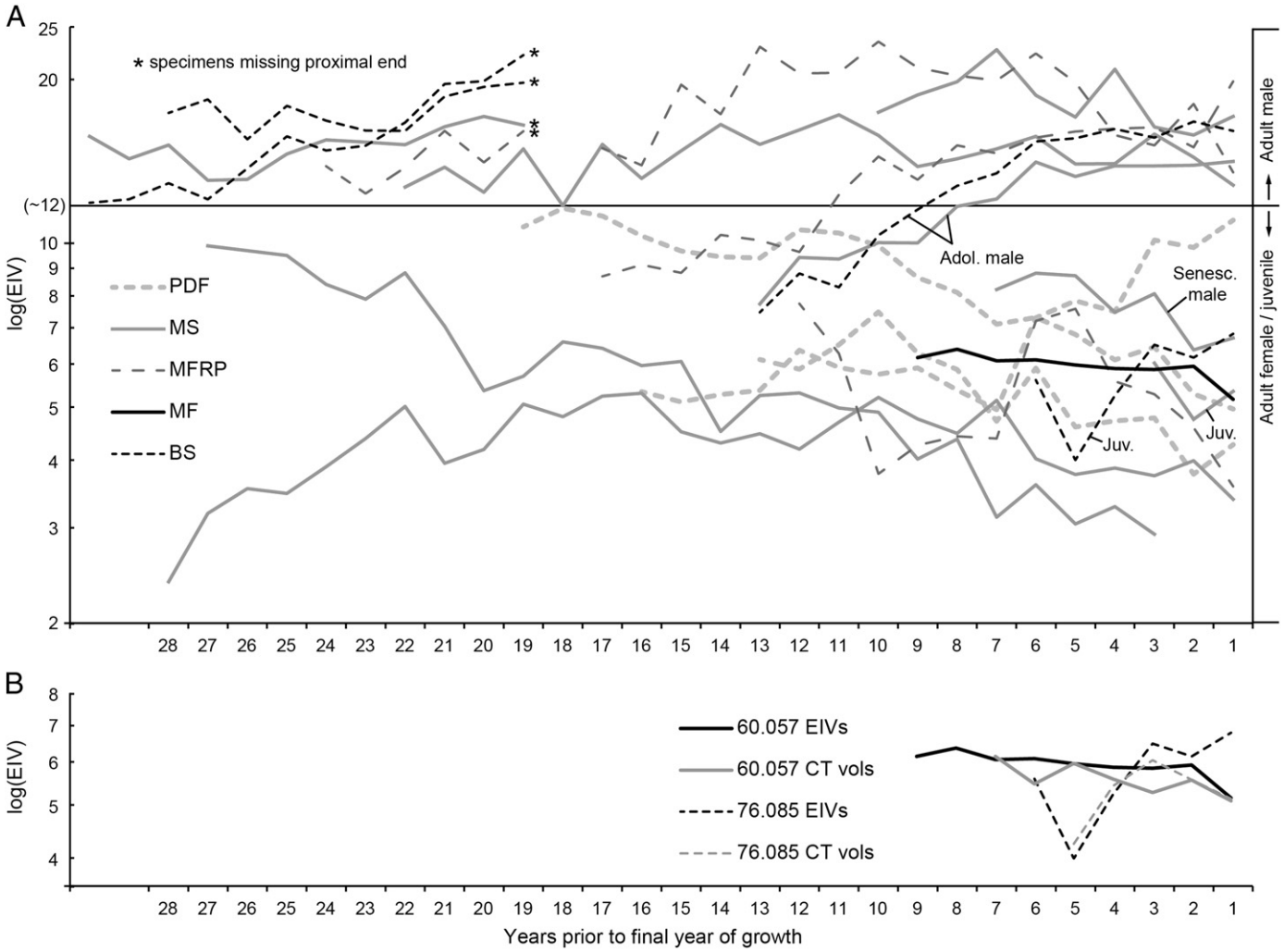

Figure 11. Growth series of estimated annual increment volumes from microCT data for ZRFS mastodon mandibular tusks. The final (incomplete) annual increment has been dropped for each series. (A) Growth series display bimodality (log scale; EIV has units of cm^3) among adult tusks indicative of sexual dimorphism. Ranges for juveniles and adult females vs. adult males are identified along right margin. Asterisks mark EIV plots for four specimens (shifted to the left side of the graph) missing their proximal end (time of death). (B) Specimens 60.057 and 76.085 show EIVs (see Fig. 3) and measured CT volumes for comparison.

would be morphologic evidence of the introgression between *M. columbi* and *M. primigenius* that left its mark in the mitogenome (Enk et al. 2011). Like the mammoths that yielded the first ancient DNA evidence of this relationship, the first ZRFS mammoths we focused on (Snowy, Clay, and the isolated teeth not discussed here) showed a more or less normal *M. columbi* phenotype. However, the three associated molars recovered late in the excavation (CCN 42–44) show definite hints of *M. primigenius* influence. However, these specimens do not include the more definitive third molars, and they still display a few features that are more consistent with *M. columbi*. We therefore formally recognize only this species as occurring at this site, but with additional material in the future, local influence of *M. primigenius* may be placed on firmer ground.

The species-level identity of ZRFS mastodons is also an intriguing problem but one whose resolution will require additional comparative treatment. The tusk configuration of ZRFS mastodons is distinctive but needs to be documented in more individuals and ideally replicated elsewhere. Another characteristic trait of ZRFS mastodons is the presence of mandibular tusks in both sexes (based on tusk diameters and growth measurements; Fig. 11). It was initially surprising to find so many mandibular tusks, because in late Pleistocene mastodons from the Midwest and Great Lakes region, they are usually present only in males and are typically lost before adulthood, although retention of mandibular tusks by adult males is known (e.g., Hay, 1914; Barbour, 1931; Skeels, 1962; Saunders, 1977). Retention in both sexes is likely the primitive condition for this lineage, but when and why did this change? Green (2006) indicated the presence of mandibular tusks in all (n = 11) Irvingtonian *M. americanum* mandibles from Florida in his study, but mandibular tusks were only present in 27% of his Rancholabrean sample (n = 22). Time binning limits the ability to track the pattern of reduced mandibular tusk occurrence through time in detail based on the Florida data. However, at the ZRFS, we now have considerable evidence that mandibular tusks were present in both sexes in the 138–113 ka interval in this region. Pinsof (1992) also noted that all mastodon mandibles from the American Falls site (Idaho, Sangamonian Stage) have mandibular tusks or alveoli.

The demographic profile of the ZRFS as a whole is notable for the abundance of young individuals and prime-age adults. Any site with this many individuals is likely to incorporate some remains derived from attritional mortality, and the partitioning of mastodon remains among and between several debris flows means that there were probably at least as many mortality events as there are stratigraphic associations. Nevertheless, the site-level demographic profile, the only data on demography we had before stratigraphic associations were sorted out, well into this research, looks more catastrophic than attritional (Klein and Cruz-Uribe, 1984; with an abundance of juveniles, adolescents, and prime-age adults). This was the initial impetus for entertaining the possibility that some distinctive entrapment mechanism might

https://doi.org/10.1016/j.yqres.2014.07.010 Published online by Cambridge University Press

have operated at the site (Cherney et al. 2012). With stratigraphic data now in hand, individual stratigraphic units show patterns similar to the whole-site pattern, with an abundance of juveniles and few or no very old individuals (Laws' Age Class > XXV). We consider briefly below how some of the evidence obtained from this site might be used to test a hypothesis of simultaneity of death for multiple individuals, but we have mostly deferred considering causes of death in favor of learning about the lives of ZRFS proboscideans and what they can tell us about their response to their environment.

Another taphonomic issue not fully resolved here is the origin of the Clay Mammoth bone/boulder association. When units 16 and 17 were being deposited (post-Bull Lake and pre-Pinedale glaciation; Pigati et al., 2014–in this volume), no glacial mechanism was available to account for postmortem transport of this assemblage. In addition, water depth at this stage in the history of the lake is unlikely to have been great enough to transport the entire assemblage in one ice-rafting event, and transport of individual boulders as dropstones fails to account for the number and concentration of carcass parts and boulders, especially against the backdrop of boulder scarcity in the broad expanse of units 16 and 17. The basin had no fluvial activity competent to displace this material, nor was there sufficient local relief to explain these elements as having slid from a higher source, even on an ice-covered surface, to the center of the basin. At present, we have no satisfactory explanation for this assemblage, but until a complete inventory and 3D model are finished, any summary statement is premature.

The most important and thoroughly investigated of the periodic features of ZRFS mastodon tusks are the radiodensity features analyzed here by microCT and recognized as marking annual increments of dentin apposition. We suspect that these are a widespread feature of tusk development that has only begun to see its full range of application. The annual nature of patterns of variation in radiodensity seems clear, and the correspondence of abrupt drops in radiodensity with periradicular bands is evidence for associating these drops with points in the annual cycle interpreted elsewhere (based on second-order increment profiles; Fisher, 1987) as winter–spring boundaries. Our thin-section studies support this interpretation, but to acquire data on more years in more individuals, our emphasis for this study has shifted from thin sections to microCT data.

Our isotopic studies were designed both as tests of the seasonal interpretation of radiodensity variation and as sources of paleobiological data in their own right. Frankly, our carbonate oxygen results were initially surprising. If radiodensity drops occur near winter–spring boundaries, tusk $\delta^{18}O$ is highest in spring and lowest during fall. This is different from expectations based on Great Lakes region mastodons, which record high values during summer and low values during winter, in agreement with regional precipitation records (e.g., Fisher, 2008; Koch et al., 1989).

However, seasonal variation in $\delta^{18}O$ of drinking water high in the Colorado Rockies might differ from expectations based on low-altitude Great Lakes locations, and relatively high $\delta^{18}O$ during winter has been documented for Colorado River discharge (Dettman et al., 2003). Possible explanations for the seasonal pattern in ZRFS tusks include seasonal migration, but we suspect that the relatively heavy oxygen values were obtained near the site because $\delta^{18}O$ series from many ZRFS tusks terminate at high values in a cycle. Moreover, our FFY results (Fig. 10) indicate that some mastodons were present in each season.

One potential cause for high winter $\delta^{18}O$ that does not require migration is ingestion of sublimated surface snowpack or meltwater derived from it. If snow provided the primary water source for ZRFS mastodons during winter, the $\delta^{18}O$ of ingested water could increase progressively as surface-snow became enriched by sublimation (Lechler and Niemi, 2011). Snowmelt during spring would initially feed runoff with enriched $\delta^{18}O$ from sublimated surface snow, but would gradually begin supplying more light oxygen as the bulk of deeper snow melted into the watershed. If summer drinking sources were fed from snowmelt and relatively light, high-altitude precipitation, heavier $\delta^{18}O$ values might return only when sublimation effects returned the next winter.

Carbonate $\delta^{13}C$ values unfortunately show evidence of diagenetic alteration, in part because they diverge from expectation for C_3 browsers, a dietary habitus documented for mastodons elsewhere (Koch et al., 1998) and corroborated here by collagen $\delta^{13}C$ values of multiple individuals and enamel carbonate $\delta^{13}C$ for one juvenile. How an oxygen isotope pattern can remain intact despite alteration of carbonate carbon isotopic composition is a question that requires additional investigation, but this is a pattern we frequently observe (e.g., Fisher and Fox, 2006). One possible explanation for the results is that these specimens, preserved in fine-grained, clay-rich sediments, may have had opportunities for isotopic exchange with only a limited volume of water in which carbonate was particularly enriched in ^{13}C, possibly as a result of methane production in the organic-rich lake basin (personal communication, K.C. Lohman, 2014). In this context, it is interesting that the record of $\delta^{13}C$ from ostracode calcite also shows evidence of enrichment and possible methane production (Sharpe and Bright, 2014–in this volume).

The cause of nitrogen isotope variation in ZRFS tusks could be seasonal changes in diet, as different plants fractionate nitrogen differently (Bocherens, 2003), but it would be difficult to predict such changes a priori. Another approach is to explain the pattern in terms of a general feature of seasonal environments. The same nitrogen isotope fractionation that elevates predator $\delta^{15}N$ by about 3‰ over tissues of their prey (DeNiro and Epstein, 1981; Gaebler et al., 1966) operates in nutritionally stressed herbivores that catabolize their own proteins in times of food shortage (Hobson et al., 1993). This results in elevated $\delta^{15}N$ for tissues produced during times of stress, such as winter (in a seasonal context, of course, stress is transient), and lower $\delta^{15}N$ in spring or early summer when new plant growth increases access to dietary protein. Seasonal climates in continental interiors might thus elicit patterns of nitrogen isotope variation like those observed in ZRFS mastodons, although ZRFS maxima (spring) and minima (fall) appear later in the year than expected, suggesting that there could be a dietary component as well. In any case, we do not observe nitrogen values that rise above the apparent seasonal norm or that are associated with any dramatic reduction in tusk growth rate, suggesting that the animals tested did not experience severe nutritional stress prior to death.

Our collagen $\delta^{13}C$ values for ZRFS mastodons are entirely consistent with the widely held understanding that this species was a predominantly C_3 feeder. These values were only “inconvenient” in that they did not vary enough on a seasonal scale to assist with our identification of seasons in the tusk record. Although our isotope analyses did not include ZRFS mammoths, we did note with interest that Pigati et al. (2014–in this volume) report a $\delta^{13}C$ value of −18.9‰ (measured in conjunction with an AMS radiocarbon age estimate) for the Clay Mammoth. This value suggests that this mammoth was also consuming mostly C_3 vegetation. Although mammoths are generally thought of as grazers, and frequently did consume C_4 vegetation, it may be that in this ecosystem, plants engaging in C_4 photosynthesis were rare.

Our report of results for the fraction of expected growth in the final year of life hinted at the seasonal identity of the radiodensity features used to discriminate years, but we return to this question now. We consider the association of abrupt radiodensity drops with periradicular bands and with a shift from thin to thicker second-order dentin increments as sufficient evidence that these features mark an approximate winter–spring boundary. We have considered our isotope results in this light, and this interpretation is not yet refuted. There is of course room for refinement of this picture, but we will proceed under this model (assignments at top of Fig. 10).

Season of death determinations were originally undertaken as a first step in evaluating the hypothesis that some entrapment mechanism might have operated at the ZRFS, explaining aspects of the demographic profile. One such mechanism is seismically induced substrate liquefaction, which has the interesting property of relating site demography and stratigraphy (the sequence of debris flows) to a common cause,

https://doi.org/10.1016/j.yqres.2014.07.010 Published online by Cambridge University Press

Table 2
Mastodon tusks from the ZRFS that were used in this study.

Field #	Sex[a]	Side[b]	Max ext. circ. (mm)[c]	Greatest length (outside curve) (mm)[c]	Medio-lateral diam. (mm)	Dorso-ventral diam. (mm)	Condition of distal end	Condition of pulp cavity	Strat[d]	μCT (# of parts)	Isotope analysis		Thin-section analysis
											Carb	Coll	
Adult mandibular tusks													
30.017	F	L?	139	152	41	46	Worn–mostly smooth	Preserved	PDF (5d)	2			
30.076	F	R	137	[215]	42	44	Missing–unworn break	Preserved	PDF (5d)	2	X		
30.130	M	L?	153	280	38	52	Worn smooth–intact	Preserved	MS (5d)	1			
33.238	F	?	128	117	35	44	Missing–partially worn	Preserved	PDF (5d)	1			
44.035	F	L	[115]	242	31	38	Worn smooth–intact	Preserved	MS (5d)	3			
45.015	M	?	167	[255]	53	52	Broken–unworn	Preserved	MS (5d)	4	X	X	
48.530	M	R	163	298	51	52	Heavily spalled–unworn	Preserved	MFRP (5d)	3	X		
48.594	M	L	155	[227]	43	54	Unworn break	Preserved	MFRP (5d)	3			
48.595	M	R	155	[167]	45	50	Worn smooth–fresh spall	Missing	MFRP (5d)	2			
56.015	F	R	129	215	34	44	Worn smooth	Preserved	MS (5d)	3	X		
58.025	M	R	161	282	49	51	Worn smooth–intact	Preserved	MS (5d)	3			
58.032	M	L	162	185	47	53	Worn smooth–intact	Missing	MS (5d)	2			
60.057	F	?	117	79	32	41	Missing–unworn break	Preserved	MF (5d)	1	X		
63.125	F	L	128	[220]	36	44	Worn smooth–intact	Preserved	MFRP (5d)	3	X		
63.170	M	L	163	[130]	47	58	Worn smooth–fresh spall	Missing	MFRP (5d)	2			
64.013	M	R	174	[150]	49	60	Worn smooth–intact	Missing	BS (5e)	2	X		
76.064	M	?	>133[e]	[165]	39	43	Missing	Missing	BS (5e)	2			
Subadult permanent mandibular tusk													
58.360	M	L	139	217	43	45	Broken–light wear	Preserved	BS (5e)	2	X	X	X
82.179	M	R	136	212	41	44	Worn–mostly smooth	Preserved	MS (5d)	2			
Juvenile permanent mandibular tusks													
56.127	J	R?	69	[117]	20	23	Worn smooth–intact	Preserved	MS (5d)	1	X		
76.085	J	R?	80	160	25	25	Worn smooth–intact	Preserved	BS (5e)	2	X		
Deciduous tusks													
17.1	J	L?	50	105	15	17	Enamel present–worn tip	Closed	PDF (5d)?	1	X		
44.146	J	L?	56	80	14	18	Enamel present–worn tip	Preserved	MS (5d)	1			
68.032	J	?	55	92	15	18	Enamel present–worn tip	Preserved	Unit 3 (5e)	1			
68.050	J	R?	64	105	17	20	Enamel present–worn tip	Preserved	BS (5e)	1	X		
71.092	J	?	60	[90]	18	20	Enamel present–worn tip	Preserved	MF (5d)	1			
77.099	J	L?	55	125	15	17	Enamel present–spalled	Closed	BS (5e)	1			
Adult premaxillary tusks													
Loc. 8	M	R	610	1730	210	170	Missing	Preserved	PDF (5d)	1	X		X
70.018	F	L	[260]	[520]	[82]	84	Broken tip–lightly worn	Preserved	MFRP (5d)	2	X	X	X
Juvenile permanent premaxillary tusk													
56.266	J	L?	126	247	38	41	Worn–mostly smooth	Preserved	MFRP (5d)	3	X		

[a] Sex determinations based on estimated increment volumes (Fig. 11); when not available, maximum circumference was used (Fig. 5).
[b] Side determinations based on general morphology and presence of attritional features often found on the medial surface.
[c] Bracketed entries in measurement columns are estimates.
[d] Stratigraphy refers to lithologic units described in Pigati et al. (2014–in this volume) for lake-margin deposits: BS, Basement Silt; MF, Main Floor; MFRP, Main Floor Red Pebble; MS, Main Silt; PDF, Primary Debris Flow. Abbreviations in parentheses follow biozone designations from Miller et al. (2014–in this volume).
[e] 76.064 is the distal tip of a large (likely male) tusk. Near the broken proximal end, its circumference is increasing, so the maximum exterior circumference must be >133 mm.

acknowledging that entrapment and dispersal of disarticulated remains implies some temporal separation of events. That is, it is clear that final deposition of ZRFS mastodon remains occurred well after death, so if one event was responsible for death, that same event could not also have figured in final transport and burial of those same remains. We have no prior expectation for how the probability of entrapment by this mechanism might relate to season, and we realize that a similar season of death does not demonstrate simultaneity of death. We nonetheless note that especially in the Main Silt and Main Floor Red Pebble units, a number of deaths occurred near the end of an annual CT increment. Perhaps this is only a reflection of higher probability of death from various causes at this time of year (Fisher, 1987), but it invites further reflection.

A better check on simultaneity of death would be serial isotope records of multiple individuals that show, or fail to show, the degree of correspondence expected for individuals that occupied the same landscape and whose last years of life were *the same years*. Figure 9B shows three such series from mandibular tusks (45.015, 48.530, 56.015) from the Main Silt and adjacent Main Floor Red Pebble layer. Although these units can be distinguished descriptively, it is less clear that they are genetically distinct. These oxygen isotope series overlap for at least the last three years of life and show remarkable consistency in overall pattern, peak values, low values, and multi-year trends. Resolving this issue is not currently our highest priority, but there are intriguing patterns that might yield to further analysis.

Whatever modes of death and postmortem transport and modification are represented at the ZRFS, the mastodon mandibular tusks preserved there are valuable archives of environmental data. They span five stratigraphic units that have been dated roughly 138 ka to 113 ka based on OSL (optically stimulated luminescence) dates on correlated sediments in lake-center deposits (Mahan et al., 2014–in this volume) and the local glacial record (Pigati et al., 2014–in this volume). This places these strata within MIS 5e and 5d, an interglacial warm period following Bull Lake alpine glaciation. Over this interval, we see a slight rise (~2‰) in average $\delta^{18}O$ values (Fig. 9A). Other things being equal, this could imply a mean annual temperature increase of 3–4°C (Dansgaard, 1964; Rozanski et al., 1993; Kohn and Welker, 2005). However, changes in precipitation and/or vapor source regions could also account for some of this difference (Koch, 1998).

Values for mean sensitivity calculated from tusk growth series change little over the MIS 5e–d interval, and are so low overall that we doubt these mastodons were seriously stressed by interannual environmental variations. To our knowledge, mean sensitivity has not been calculated for other mammalian accretionary growth structures, so the published values with which we can make comparisons are limited. For tree-ring data, there is a conventional threshold (0.30) for distinguishing "complacent" and "sensitive" responses (Creber, 1977). Black (2009) reported mean sensitivities of 0.15 to 0.20 for fish otolith growth series and 0.22 to 0.29 for growth series from geoduck valves that appeared responsive to environmental variations. Additionally, Butler et al. (2013) gave a value of 0.499 for shell growth series of *Arctica islandica*, a relatively sensitive bivalve species often used for marine climate reconstructions. The average for all adult ZRFS tusk series (0.08) is low in comparison to values from growth structures in these ectotherms, but it is also lower than values we calculated for two mastodon premaxillary tusks from late Pleistocene sites in New York (Fisher, 2008; Fisher et al., 2008; Supp. Table 1). That ZRFS mastodons were not facing significant stress is further supported by the relatively low $\delta^{15}N$ values we measured. Higher in the section, mastodons are replaced by mammoths, implying that the change to MIS 4 eventually elicited a range shift, requiring us to pick up the mastodon story at other sites. We originally hoped to be able to track more of the history of environmental change at this one site, and we have a few options (including specimens in the Beach Silt, not represented by mandibular tusks) for extending our analyses both up- and down-section, but a longer-term perspective may require broader geographic as well as stratigraphic integration.

Conclusions

The Ziegler Reservoir fossil site is noteworthy in producing a large number of well-preserved mandibular tusks of late Pleistocene mastodons. This study represents a first attempt to use American mastodon mandibular tusks to assess individual life histories and environmental change at a single site. Given the time range sampled, this site provides more than the usual "snapshot" of an ancient ecosystem, but we still only get a series of snapshots, or a short "video clip," of the response to longer-term patterns of climate change. The most promising results are that mandibular tusks offer a compact record extending sometimes through decades of life, and microCT analyses represent an effective means of gathering data on tusk growth rates that should act as sensitive indicators of environmental conditions. Mastodons inhabiting alpine regions of central Colorado between ~140 and 110 ka appear to have thrived within a highly seasonal interglacial environment. Some of our methods for studying their paleobiology may translate effectively to studies of mastodon response to even later changes in the Pleistocene, closer to the time of their extinction.

Supplementary data to this article can be found online at http://dx.doi.org/10.1016/j.yqres.2014.07.010.

Acknowledgments

We thank Kirk Johnson and Ian Miller for organizing the Snowmastodon Project and inviting our participation. Specimens referenced in this paper were collected at the Ziegler Reservoir locality, 5PT1264, under State of Colorado Paleontological Permits 2010–106 and 2011–17. The authors thank History Colorado/the Colorado Historical Society, the Snowmass Water and Sanitation District, and the Town of Snowmass Village for assistance with this excavation and the USGS for LiDAR scans of the Clay Mammoth. DMNS provided support for analyses. We also acknowledge the work of many volunteers in site excavation, and Rick Wicker and Scott Beld for specimen photography.

References

Agenbroad, L.D., 1994. Taxonomy of North American *Mammuthus* and biometrics of the Hot Springs mammoths. In: Agenbroad, L.D., Mead, J.I. (Eds.), The Hot Springs Mammoth Site. The Mammoth Site, Hot Springs, South Dakota, pp. 158–207.

Barbour, E.H., 1931. The American mastodon with mandibular tusks. Nebraska State Museum Bulletin 19 (1), 163–170.

Black, B.A., 2009. Climate-driven synchrony across tree, bivalve, and rockfish growth-increment chronologies of the northeast Pacific. Marine Ecology Progress Series 378, 37–46.

Bocherens, H., 2003. Isotopic biogeochemistry and the paleoecology of the mammoth steppe fauna. In: Reumer, J.W.F., de Vos, J., Mol, D. (Eds.), Advances in Mammoth Research. Deinsea. 9, pp. 57–76.

Bunn, A.G., 2008. A dendrochronology program library in R (dplR). Dendrochronologia 26, 115–124.

Butler, P.G., Wanamaker, A.D., Scourse, J.D., Richardson, C.A., Reynolds, D.J., 2013. Variability of marine climate on the North Icelandic Shelf in a 1357-year proxy archive based on growth increments in the bivalve *Arctica islandica*. Palaeogeography, Palaeoclimatology, Palaeoecology 373, 141–151.

Cherney, M.D., Fisher, D.C., Rountrey, A.N., Calamari, Z.T., 2012. Isotope analyses support use of CT scans for identifying annual increments in Snowmass mastodon mandibular tusks. Journal of Vertebrate Paleontology, Supplement, 72nd Annual Meeting, Program and Abstracts. 77.

Cook, E.R., Peters, K., 1981. The smoothing spline: a new approach to standardizing forest interior tree-ring width series for dendroclimatic studies. Tree-Ring Bulletin 41, 45–53.

Creber, G.T., 1977. Tree rings: a natural data-storage system. Biological Reviews 52, 349–383.

Dansgaard, W., 1964. Stable isotopes in precipitation. Tellus 16, 436–468.

DeNiro, M.J., 1985. Postmortem preservation and alteration of in vivo bone collagen isotope ratios in relation to palaeodietary reconstruction. Nature 317, 806–809.

DeNiro, M.J., Epstein, S., 1981. Influence of diet on the distribution of nitrogen isotopes in animals. Geochimica et Cosmochimica Acta 45, 341–351.

Dettman, D.L., Flessa, K.W., Roopnarine, P.D., Schöne, B.R., Goodwin, D.H., 2003. The use of oxygen isotope variation in shells of estuarine mollusks as a quantitative record of

seasonal and annual Colorado River discharge. Geochimica et Cosmochimica Acta 69, 1253–1263.
Douglass, A.E., 1920. Evidence of climatic effects in the annual rings of trees. Ecology 1, 24–32.
Enk, J., Debruyne, R., Devault, A., King, C.E., Treangen, T., O'Rourke, D., Slazberg, S.L., Fisher, D., MacPhee, R., Poinar, H., 2011. Complete Columbian mammoth mitogenome suggests interbreeding with woolly mammoths. Genome Biology 12 (R51), 1–8. http://dx.doi.org/10.1186/gb-2011-12-5-r51.
Falconer, H., 1857. On the species of mastodon and elephant occurring in the fossil state in Great Britain. Part 1. *Mastodon*. Quarterly Journal of the Geological Society of London 13, 307–360.
Fisher, D.C., 1987. Mastodont procurement by Paleoindians of the Great Lakes region: hunting or scavenging? In: Nitecki, M.H., Nitecki, D.V. (Eds.), The Evolution of Human Hunting. Plenum Press, New York, pp. 309–421.
Fisher, D.C., 1988. Season of death of the Hiscock mastodonts. In: Laub, R.S., Miller, N.G., Steadman, D.W. (Eds.), Late Pleistocene and Early Holocene Paleoecology and Archaeology of the Eastern Great Lakes Region. Bulletin of the Buffalo Society of Natural Sciences. 33, pp. 115–125.
Fisher, D.C., 1996. Extinction of proboscideans in North America. In: Shoshani, J., Tassy, P. (Eds.), The Proboscidea: Evolution and Palaeoecology of Elephants and Their Relatives. Oxford University Press, Oxford, pp. 296–315.
Fisher, D.C., 2008. Taphonomy and paleobiology of the Hyde Park mastodon. In: Allmon, W.D., Nester, P.L. (Eds.), Mastodon Paleobiology, Taphonomy, and Paleoenvironment in the Late Pleistocene of New York State: Studies on the Hyde Park, Chemung, and North Java Sites. Palaeontographica Americana. 61, pp. 197–290.
Fisher, D.C., 2009. Paleobiology and extinction of proboscideans in the Great Lakes region of North America. In: Haynes, G. (Ed.), American Megafaunal Extinctions at the End of the Pleistocene. Springer, Dordrecht, pp. 55–75.
Fisher, D.C., Fox, D.L., 2003. Season of death and terminal growth histories of Hiscock mastodons. In: Laub, R.S. (Ed.), The Hiscock Site: Late Pleistocene and Holocene Paleoecology and Archaeology of Western New York State. Bulletin of the Buffalo Society of Natural Sciences. 37, pp. 83–101.
Fisher, D.C., Fox, D.L., 2006. Five years in the life of an Aucilla River mastodon. In: Webb, S.D. (Ed.), First Floridians and Last Mastodons: The Page–Ladson Site in the Aucilla River. Springer, Dordrecht, pp. 343–377.
Fisher, D.C., Beld, S.G., Rountrey, A.N., 2008. Tusk record of the North Java mastodon. In: Allmon, W.D., Nester, P.L. (Eds.), Mastodon Paleobiology, Taphonomy, and Paleoenvironment in the Late Pleistocene of New York State: Studies on the Hyde Park, Chemung, and North Java Sites. Palaeontographica Americana. 61, pp. 417–463.
Fritts, H.C., 1976. Tree Rings and Climate. Academic Press, New York, (567 pp.).
Gaebler, O.H., Vitti, T.G., Vukmirovich, R., 1966. Isotope effects in metabolism of ^{14}N and ^{15}N from unlabeled dietary proteins. Canadian Journal of Biochemistry 44, 1249–1257.
Graham, R., 1986. Descriptions of the dentitions and stylohyoids of *Mammuthus columbi* from the Colby Site. In: Frison, G.C., Todd, L.C. (Eds.), The Colby Mammoth Site: Taphonomy and Archaeology of a Clovis Kill in Northern Wyoming. University of New Mexico Press, Albuquerque, pp. 171–190.
Green, J.L., Hulbert Jr., R.C., 2006. The deciduous premolars of *Mammut americanum* (Mammalia, Proboscidea). Journal of Vertebrate Paleontology 25, 702–715.
Hay, O.P., 1914. The Pleistocene mammals of Iowa. Iowa Geological Survey Annual Reports 23, 1–662.
Haynes, G., 1991. Mammoths, Mastodonts, and Elephants. Cambridge University Press, Cambridge, (413 pp.).
Hobson, K.A., Alisauskas, R.T., Clark, R.G., 1993. Stable-nitrogen isotope enrichment in avian tissues due to fasting and nutritional stress: implications for isotopic analysis of diet. The Condor 95, 388–394.
Kerr, R., 1792. The Animal Kingdom or Zoological System, of the Celebrated Sir Charles Linnaeus …, London [Complete Citation, Together with C. Linnaeus and J.F. Gmelin, in Osborn, H.F., 1936. Proboscidea. The American Museum Press, New York, p. 782].
Klein, R.G., Cruz-Uribe, K., 1984. The Analysis of Animal Bones from Archaeological Sites. The University of Chicago Press, Chicago, (xii + 266 pp.).
Koch, P.L., 1998. Isotopic reconstruction of past continental environments. Annual Review of Earth and Planetary Sciences 26, 573–613.
Koch, P.L., Fisher, D.C., Dettman, D., 1989. Oxygen isotope variation in the tusks of extinct proboscideans: a measure of season of death and seasonality. Geology 17, 515–519.
Koch, P.L., Fogel, M.L., Tuross, N., 1994. Tracing the diets of fossil animals using stable isotopes. In: Lajtha, K., Michener, B. (Eds.), Stable Isotopes in Ecology and Environmental Science. Blackwell Scientific Publications, Oxford, pp. 63–92.
Koch, P.L., Tuross, N., Fogel, M.L., 1997. The effects of sample treatment and diagenesis on the isotopic integrity of carbonate in biogenic hydroxylapatite. Journal of Archaeological Science 24, 417–429.
Koch, P.L., Hoppe, K.A., Webb, S.D., 1998. The isotopic ecology of late Pleistocene mammals in North America, Part 1. Florida. Chemical Geology 152, 119–138.
Kohn, M.J., Welker, J.M., 2005. On the temperature correlation of $\delta^{18}O$ in modern precipitation. Earth and Planetary Science Letters 231, 87–96.
Laws, R.M., 1966. Age criteria for the African elephant, *Loxodonta a. africana*. East African Wildlife Journal 4, 1–37.
Laxson, T.A., 2011. Geospatial Analysis of Mean Sensitivity in *Pinus strobus*. M.A. dissertation The University of North Carolina at Greensboro, (121 pp.).
Lechler, A.R., Niemi, N.A., 2011. The influence of snow sublimation on the isotopic composition of spring and surface waters in the southwestern United States: implications for stable isotope-based paleoaltimetry and hydrologic studies. Geological Society of America Bulletin 124 (3/4), 318–334.
Maglio, V.J., 1973. Origin and evolution of the *Elephantidae*. Transactions of the American Philosophical Society, New Series 63, 1–149.
Mahan, S.A., Gray, H.J., Pigati, J.S., Wilson, J., Lifton, N.A., Paces, J., Blaauw, M., 2014. A geochronologic framework for the Ziegler Reservoir fossil site, Snowmass Village, Colorado. Quaternary Research 82, 490–503 (in this volume).
Miller, I.M., Pigati, J.S., Anderson, R.S., Johnson, K.R., Mahan, S.A., Ager, T.A., Baker, R.G., Blaauw, M., Bright, J., Brown, P.M., Bryant, B., Calamari, Z.T., Carrara, P.E., Cherney, M.D., Demboski, J.R., Elias, S.A., Fisher, D.C., Gray, H.J., Haskett, D.R., Honke, J.S., Jackson, S.T., Jiménez-Moreno, G., Kline, D., Leonard, E.M., Lifton, N.A., Lucking, C., McDonald, H.G., Miller, D.M., Muhs, D.R., Nash, S.E., Newton, C., Paces, J.B., Petrie, L., Plummer, M.A., Porinchu, D.F., Rountrey, A.N., Scott, E., Sertich, J.J.W., Sharpe, S.E., Skipp, G.L., Strickland, L.E., Stucky, R.K., Thompson, R.S., Wilson, J., 2014. A high-elevation, multi-proxy biotic and environmental record of MIS 6–4 from the Ziegler Reservoir fossil site, Snowmass Village, Colorado USA. Quaternary Research 82, 618–634 (in this volume).
Pigati, J.S., Miller, I.M., Johnson, K.R., Honke, J.S., Carrara, P.E., Muhs, D.R., Skipp, G., Bryant, B., 2014. Geologic setting and stratigraphy of the Ziegler Reservoir fossil site, Snowmass Village, Colorado. Quaternary Research 82, 477–489 (in this volume).
Pinsof, J.D., 1992. The Late Pleistocene Vertebrate Fauna from the American Falls Area, Southeastern Idaho. Ph.D. dissertation Idaho State University, (399 pp.).
Rountrey, A.N., 2009. Life Histories of Juvenile Woolly Mammoths from Siberia: Stable Isotope and Elemental Analyses of Tooth Dentin. Unpublished dissertation University of Michigan, (xiii + 331 pp.).
Rountrey, A.N., Fisher, D.C., Vartanyan, S., Fox, D.L., 2007. Carbon and nitrogen isotope analyses of a juvenile woolly mammoth tusk: evidence of weaning. Quaternary International 169–170, 166–173.
Rozanski, K., Araguás-Araguás, L., Gonfiantini, R., 1993. Isotopic patterns in modern global precipitation. In: Swart, J.P., Lohmann, K.C., McKenzie, J., Savin, S. (Eds.), Climate Change in Continental Isotopic Records. American Geophysical Union, Geophysical Monograph. 78, pp. 1–36.
Saunders, J.J., 1970. The Distribution and Taxonomy of *Mammuthus* in Arizona. Unpublished M.S. thesis University of Arizona, (115 pp.).
Saunders, J.J., 1977. Late Pleistocene vertebrates of the western Ozark Highland, Missouri. Illinois State Museum Reports of Investigations 33, 1–118.
Sharpe, S.E., Bright, J., 2014. A high-elevation MIS 5 hydrologic record using mollusks and ostracodes from Snowmass Village, Colorado, USA. Quaternary Research 82, 604–617 (in this volume).
Skeels, M.A., 1962. The mastodons and mammoths of Michigan. Michigan Academy of Science, Arts, and Letters, Papers 47, 101–133.
Smith, K.M., Fisher, D.C., 2011. Sexual dimorphism of structures showing indeterminate growth: tusks of American mastodons (*Mammut americanum*). Paleobiology 37, 175–194.
Trapani, J., Fisher, D.C., 2003. Discriminating proboscidean taxa using features of the Schreger pattern in tusk dentin. Journal of Archaeological Science 30, 429–438.

https://doi.org/10.1016/j.yqres.2014.07.010 Published online by Cambridge University Press